Journal of Asian Earth Sciences 88 (2014) 230–245

Contents lists available at ScienceDirect

Journal of Asian Earth Sciences

journal homepage: www.elsevier.com/locate/jseaes

How fast is the denudation of the Taiwan mountain belt? Perspectives from in situ cosmogenic ^{10}Be

Florence Derrieux [a], Lionel L. Siame [a,b,f,*], Didier L. Bourlès [a,f], Rou-Fei Chen [c,f], Régis Braucher [a,f], Laetitia Léanni [a], Jian-Cheng Lee [c,f], Hao-Tsu Chu [d,f], Timothy B. Byrne [e]

[a] Aix-Marseille Université, CNRS-IRD-Collège de France, UM 34 CEREGE, Technopôle de l'Arbois, BP80, 13545 Aix-en-Provence, France
[b] Institute of Earth Sciences, Academia Sinica, 128 Academia Road Sec. 2, Nankang, Taipei 115, Taiwan
[c] Department of Geology, Chinese Culture University, 55, Hwa-Kang Road, Yang-Ming-Shan, Taipei, Taiwan
[d] Central Geological Survey, Ministry of Economic Affairs, P.O. Box 968, Taipei, Taiwan
[e] Center for Integrative Geosciences, University of Connecticut, Storrs, CT 06269, United States
[f] LIA (Associated International Laboratory), ADEPT (Active Deformation and Environment Programme for Taiwan), Centre National de la Recherche Scientifique/Institut National des Sciences de l'Univers (France), National Science Council, Taiwan

ARTICLE INFO

Article history:
Received 18 September 2013
Received in revised form 27 February 2014
Accepted 17 March 2014
Available online 29 March 2014

Keywords:
Denudation
Cosmogenic nuclides [^{10}Be]
Mountain building
Taiwan

ABSTRACT

Quantifying denudation rates in a wide range of climatic and tectonic settings at various time and space scales is a critical step in calibrating and validating landscape evolution models. Focusing on Taiwan, we quantified centennial rates of denudation at the scale of the whole orogen, using in situ ^{10}Be concentrations measured in stream sediments collected at the outlets of major rivers. To assess denudation rates that are statistically significant, we applied both the mean square weighted deviation approach and the bootstrap technique. For the central segment of the belt, where the collision is considered to be near mature, the orogen-scale pattern of denudation shows a two-fold pattern: (1) higher denudation values on the order of 4–5 mm/yr characterize the eastern side of the belt (i.e., retro-wedge), with a slight increase towards the south and (2) lower denudation values on the order of 1–3 mm/yr on the western side of the belt (pro-wedge) with a minimum value centered on the main recess of the deformation front. To the north and to the south of the central segment, the denudation rates converge towards lower values on the order of 2–3 mm/yr. At the scale of the mountain belt, drainage basin metrics such as relief, hypsometric index and slope values seem to explain the observed variance in the data population, conversely to the first-order average precipitation pattern, suggesting a strong tectonic control on the regional pattern of denudation rates. Applied to the whole orogen, such field-based approach thus provides important input data to validate and calibrate the parameters to be supplied to landscape evolution models.

1. Introduction

Orogenic settings resulting from tectonic evolution along convergent margins record connection between deep and surface processes (Davis et al., 1983; Selzer et al., 2008). Within orogenic wedges, horizontal and vertical tectonic movements indeed create a topographic relief that is in turn progressively destroyed by denudational processes (Willett, 1999), leading to landmass redistributions (Konstantinovskaia and Malavieille, 2005). Nevertheless, the interaction of deep and shallow processes is still poorly understood and the role these processes play in the exhumation of rocks, in the structural evolution of orogenic wedges, and in defining the relations between tectonics and climate-dependent surface processes are still debated (Dahlen and Suppe, 1988; Whipple and Meade, 2004; Cruz et al., 2010; Konstantinovskaya and Malavieille, 2011). However, as pointed out by Molnar (2009), it may be more pertinent to quantify independently the processes involved in mountain belt evolution rather than trying to study the interactions among them. As part of this effort, quantification of denudation rates in a wide range of climatic and tectonic settings at various time and space scales is a critical step in providing fundamental input parameters to feed analog and numerical models of orogenic systems.

The present-day denudational context of Taiwan is controlled by high uplift rates (e.g., Ching et al., 2011), linked to the northwest-directed collision of the north-trending Luzon arc against

* Corresponding author at: Aix-Marseille Université, CNRS-IRD-Collège de France, UM 34 CEREGE, Technopôle de l'Arbois, BP80, 13545 Aix-en-Provence, France and Institute of Earth Sciences, Academia Sinica, 128 Academia Road Sec. 2, Nankang, Taipei 115, Taiwan. Tel.: +33 442 971 760.
E-mail address: siame@cerege.fr (L.L. Siame).

http://dx.doi.org/10.1016/j.jseaes.2014.03.012
1367-9120/

the northeast-trending continental margin of Eurasia at a rate of roughly 82 mm/yr (Yu et al., 1997; Sella et al., 2002). Combined with a tropical to sub-tropical climate characterized by mean annual precipitations on the order of 2500 mm and an average of four typhoons per year hitting the island, this geodynamic situation has led to a high, deeply incised topography, triggering the evolution of the wedge towards a state of quasi-equilibrium in which input and output processes are considered to be balanced (e.g., Koons, 1990; Beaumont et al., 2000; Suppe, 1981; Dahlen and Suppe, 1988; Willett et al., 2003; Molnar, 2009).

In Taiwan, denudation is essentially accomplished by runoff on hillslopes and transport by rivers with a strong predominance of suspended and bed load fractions (Lee, 1976; Li et al., 2005), and landslides that break away rock masses and promote rapid outgoing sedimentary fluxes by the rivers (Hovius et al., 2000; Chen et al., 2005). In Taiwan, denudation rates have been estimated by methodological approaches spanning a few decades, using suspended load data from major rivers (Lee, 1976; Dadson et al., 2003; Fuller et al., 2003; Li et al., 2005; Siame et al., 2011), to a few millions of years, using data from low-temperature thermochronology and associated thermo-mechanical models (Liu, 1982; Liu et al., 2000; 2001; Willett et al., 2003; Fuller et al., 2006; Simoes et al., 2007; Beyssac et al., 2007) or using detrital pyrrhotite mineral distribution (Horng et al., 2012). The first group of studies involves calibrations linking water discharge and river suspended load (Lee, 1976), coupled with stochastic modeling of the hydrological signal temporal variations (Fuller et al., 2006) or with estimation of the bed load component (Dadson et al., 2003). These approaches estimated average denudation rates ranging from 2 to 8 mm/yr in the Central Range, and on the order of 5 mm/yr for the whole mountain belt of Taiwan, with local maximum values exceeding 30 mm/yr (Dadson et al., 2003). This average value of 5 mm/yr is close to that obtained by You et al. (1988) using the concentration of atmospheric cosmogenic ^{10}Be in river sediments.

The second group of studies relies on fission track data, which yield long-term rates of exhumation on the order of 3–6 mm/yr for the Central Range (Liu, 1982; Liu et al., 2000, 2001; Dadson et al., 2003; Willett et al., 2003). However, recent reassessment using fission track data combined with two-dimensional thermo-mechanical models including heat flux calibrations (Fuller et al., 2006; Simoes et al., 2007; Yamato et al., 2009) proposed lower long-term rates of denudation throughout the whole orogen ranging between 2 and 4 mm/yr for the Taiwan mountain belt. Using pyrrhotite mineral as a tracer for denudation of the Taiwan orogeny, Horng et al. (2012) proposed that the exhumation and the denudation of the belt accelerated since the late Pliocene from less than 1 mm/yr to more than 2 mm/yr, that generally agrees with the onset timing of the arc-collision in Taiwan.

Even if, at the scale of the whole orogen, the denudation rates estimated from these different techniques roughly converge towards values on the order of 3–5 mm/yr, it appears difficult to derive a more precise pattern at the regional or more local scale. On the one hand, the denudation rates derived from decadal suspended loads could be significantly imprinted by the extreme processes resulting from landslides triggered by typhoons and earthquakes, as well as biased by the poor control on the bed load contribution to the sediment out flux (e.g., Dadson et al., 2003; Li et al., 2005; Siame et al., 2011). With values higher than 30 mm/yr in some parts of the Taiwan orogen, such denudation rates can hardly be regarded as representative for longer geological time scales (see Fig. 2a in Dadson et al., 2003). On the other hand, if the thermo-chronological models provide insight into behavior of conceptual orogenic systems, the thermal history of the Taiwan collision may not be a steady process and, therefore, the derived long-term rates of denudation should be considered with caution.

In this study, we investigate the rates at which the topography of the Taiwan mountain range is being eroded. To achieve this goal, we quantified spatially averaged denudation rates determined from in situ-produced cosmogenic ^{10}Be concentrations measured in river-borne quartz grains and conducted a statistical analysis to determined the best representative central values for nine major watersheds located on both sides of the Taiwan orogen. This analysis allows examining the pattern and magnitude of denudation rates at the scale of the orogenic system, which provides the necessary data for interpreting the denudational conditions that prevail in the Taiwan mountain belt. Hereafter, we first present the rational for determining denudation rates from measurement of in situ produced ^{10}Be in detrital river sediment and its application to Taiwan's watersheds. We then detail the data analysis in terms of reliability of the data, identification of outliers and search of meaningful central values to characterize the denudation rate prevailing within each studied watershed. Finally, we gauge the cosmogenic-derived denudation rates against geomorphic metrics and discuss the regional pattern of denudation rates.

2. Cosmogenic-derived denudation rates

Secondary particles, derived from nuclear reactions produced by cosmic rays within the atmosphere, interact with rocks or soils exposed at the Earth's surface, producing ^{10}Be predominantly within a few meters below the surface because of the exponential attenuation of production rates with depth (Lal, 1991; Gosse and Phillips, 2001). In situ-produced cosmogenic ^{10}Be concentrations measured in river-borne sands can be used to document hillslope exposure history and estimate basin averaged denudation rates (Brown et al., 1995a; Bierman and Steig, 1996; Granger et al., 1996). The cosmogenic build-up records hillslope denudation history while the material is vertically mixed-up through the upper meters of regolith, and thus integrates both the erosional and weathering processes associated with surface denudation. Since the rivers carry and mix the sediment derived from the soil-mantled hillslopes, they are natural spatial integrators of these processes. Assuming cosmogenic production steady state and negligible transport time at the surface, determination of ^{10}Be concentrations in river-borne quartz allows estimating time-integrated rates of denudation at the basin scale (for reviews, see von Blanckenburg, 2005; Granger and Riebe, 2013; Granger et al., 2013). In landscapes evolving significantly through mass-wasting processes such as Taiwan, the changes in sediment fluxes following landslides make the sediment residence time in the system more variable (Yanites et al., 2009). Nevertheless, previous studies using numerical modeling (e.g., Niemi et al., 2005), suggest that larger catchments are likely to yield a better approximation of long-term denudation rate than smaller catchments and that sampling multiple, similarly-sized watersheds also have a significant likelihood of yielding consistent cosmogenic-derived denudation rates.

In an effort to document the regional pattern and magnitude of denudation rates throughout the Taiwan mountain belt, nine main river catchments and some associated sub-basins (with areas larger than 50 km^2) have been sampled from north to south and on both sides of the orogen (Fig. 1). A total of 33 samples, each consisting of ~2 kg of stream sand collected in the active riverbed, were collected. For some sites, quartz pebbles were also sampled providing the opportunity to compare denudation rate estimations for two very different grain sizes. In online Supplemental material (hereafter referred as Appendix A), we provide location and field photographs for each sampled watershed.

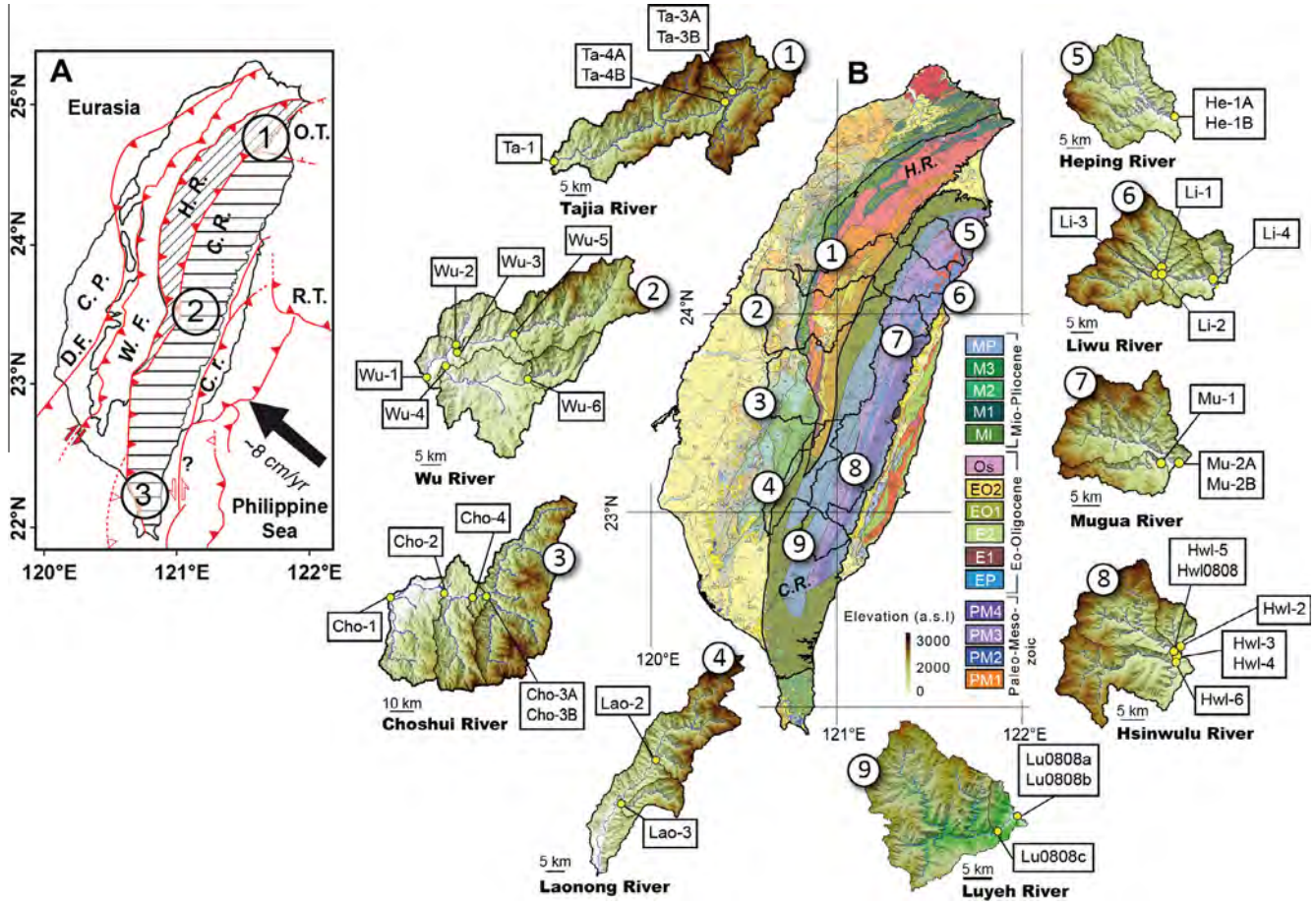

Fig. 1. Localization of the studied watersheds. (A) Structural domains of Taiwan: C.P., Coastal Plain; W.F., Western Foothills; H.R., Hsueshan Range; C.R., Central Range; C.R., Coastal Range; O.T., Okinawa Trough; R.T., Ryukyu Trench; D.F., Deformation Front. Circled numbers refer to the different collision stages: (1: waning; 2: mature; 3: incipient continental subduction) after Shyu et al. (2005). (B) Geological map of Taiwan (Chen et al., 2009) locating the studied catchments. Circled numbers refer to the watersheds displayed around the map. Inserts show the topography of the studied watersheds with sample locations (elevation in meters above sea level from a 40 m-resolution digital elevation model). MI, Miocene argilites, slate, phyllite; Ep, Eocene slate, phyllite; PM4, Paleozoic–Mesozoic black schist; PM3, Black schist, greenschist, siliceous schist; PM2, Metamorphosed limestone; PM1, Gneiss and migmatite.

2.1. Sample preparation

Chemical treatments and preparations for Accelerator Mass Spectrometry (AMS) measurements were performed at the Laboratoire National des Nucléides Cosmogéniques (LN2C) housed by CEREGE (Aix en Provence, France), following chemical procedures adapted from Brown et al. (1991) and Merchel and Herpers (1999). After sieving, the 1–0.25 mm fraction was separated into magnetic and non-magnetic fractions, and the non-magnetic fraction was bathed in fluorosilicic and hydrochloric acids to eliminate all mineral phases except quartz. The quartz minerals then underwent a series of selective etchings in hydrofluoric acid to eliminate potential surface contamination by ^{10}Be produced in the atmosphere. The cleaned quartz minerals were then completely dissolved in hydrofluoric acid after addition in each sample of ~100 µl of an in-house carrier solution (3.025 ± 0.009) $\times 10^{-3}$ g ^{9}Be/g solution) prepared from a deep-mined phenakite crystal (Merchel et al., 2008). Hydrofluoric and Perchloric fuming was used to remove fluorides and both cation and anion exchange chromatography were used to eliminate iron, aluminum, manganese and other elements. Beryllium oxide was mixed to 325 mesh niobium powder prior to measurements by Accelerator Mass Spectrometry (AMS), which were performed at ASTER (Accélérateur pour les Sciences de la Terre, Environnement et Risques, Aix-en-Provence) AMS French facility (Arnold et al., 2010). Beryllium-10 data were calibrated directly versus the National Institute of Standards and Technology standard reference material NIST SRM 4325 using an assigned ^{10}Be/^{9}Be value of (2.79 ± 0.03) $\times 10^{-11}$ (Nishiizumi et al., 2007) and a ^{10}Be half-life of (1.387 ± 0.012) $\times 10^{6}$ years (Korschinek et al., 2010; Chmeleff et al., 2010).

2.2. Basin-wide denudation rates

To determine basin averaged production rates, scaling factors for latitude and altitude corrections were calculated according to Stone (2000), for each pixel of a 40 m-resolution digital elevation model (DEM) using the Cronus-Earth Matlab scripts (http://hess.ess.washington.edu/math/). Geomorphic shielding factors were also calculated for each pixel of the DEM using a 10° azimuth step following formulations by Dunne et al. (1999). For the eastern watersheds, surfaces corresponding to outcrops of carbonate lithologies have been masked, removing their contribution from the total production rate and allowing only for the areas with quartz-bearing rocks (Table 1). For each sampled watersheds, basin averaged production rates were calculated using a modern ^{10}Be production rate at sea level and high latitude of 4.5 ± 0.3 atoms/g-SiO_2/yr to account for the reevaluation of absolute calibration of ^{10}Be AMS standards proposed by Nishiizumi et al. (2007). Sample information as well as ^{10}Be concentrations are presented in Table 1.

Table 1
Sampling location, watershed characteristics and Accelerator Mass Spectrometry (AMS) measurements performed at ASTER (Accélérateur pour les Sciences de la Terre, Environnement et Risques, Aix-en-Provence) AMS French facilities (Arnold et al., 2010).

Watershed	Sample ID	Grain size	Basin area (km^2)[a]		Mean elevation (m)	Sample location (WGS84)		$^{10}Be/^{9}Be$[b]				[$^{10}Be/^{9}Be$] (10^3 atoms/g)[d]		Scaling factor[e]		Scaled mean production rates (at./g/yr)[f]		
			Total	Reduced		Lat. (°N)	Lon (°E)	Value ($\times 10^{-15}$)	Error (%)	N	Chi-square[c]	Value	Error	Shielding	Stone's factor	Neutrons	Slow muons	Fast muons
Western side																		
Tajia (1)	Ta-1	Sand	964	–	2094	24.16	120.85	4.96	12.8	66	31.57	6.81	1.17	0.95	3.65	15.61	0.03	0.06
	Ta-2	Sand	257	–	2467	24.3	121.27	7.25	52.1	4	3.08	–	–	–	–	–	–	–
	Ta-3A	Sand	155	–	2438	24.32	121.28	2.9	19.4	27	10.33	10.91	3.25	0.95	4.39	18.79	0.03	0.06
	Ta-3B	Pebbles	155	–	2438	24.32	121.28	3.92	16.89	43	17.35	3.05	0.71	0.95	4.39	18.79	0.03	0.06
	Ta-4A	Sand	418	–	2444	24.3	121.26	3.75	21.32	22	11.92	11.81	3.33	0.96	4.38	18.85	0.03	0.06
	Ta-4B	Pebbles	418	–	2444	24.3	121.26	3.51	12.5	64	21.58	2.47	0.5	0.96	4.38	18.85	0.03	0.06
Wu (2)	Wu-1	Sand	996	–	1073	23.99	120.8	6.11	12.22	67	40.11	9.13	1.4	0.97	1.82	7.92	0.02	0.05
	Wu-2	Sand	78	–	716	24.05	120.86	6.51	11.79	72	44.28	5.6	0.82	0.98	1.29	5.73	0.02	0.05
	Wu-3	Sand	435	–	1464	24.05	120.86	3.75	13.02	59	22.64	8.34	1.66	0.95	2.4	10.27	0.02	0.05
	Wu-4	Sand	420	–	824	24.02	120.84	20.83	5.93	341	237.08	24.49	1.57	0.98	1.43	6.3	0.02	0.05
	Wu-5	Sand	337	–	1676	24.08	120.98	4.32	12.74	66	27.54	5.2	0.95	0.95	2.71	11.53	0.02	0.05
	Wu-6	Sand	98	–	1265	23.99	121.01	7.07	22.27	27	15.73	9.48	2.37	0.96	1.96	8.45	0.02	0.05
Choshui (3)	Cho-1	Sand	2892	–	1554	23.79	120.63	4.38	12.81	61	27.74	4.13	0.75	0.96	2.64	11.38	0.02	0.05
	Cho-2	Sand	2196	–	1782	23.81	120.84	5.45	10.84	87	42.72	5.97	0.88	0.95	3	12.85	0.02	0.05
	Cho-3A	Sand	1486	–	1997	23.79	121	2.91	13.25	57	15.39	3.12	0.74	0.95	3.38	14.45	0.03	0.06
	Cho-3B	Pebbles	1486	–	1997	23.79	121	2.45	15.43	42	10.07	1.17	0.34	0.95	3.38	14.45	0.03	0.06
	Cho-4	Sand	1537	–	1974	23.79	120.93	11.85	9.17	119	91.57	9.39	0.97	0.95	3.34	14.26	0.03	0.06
Laonong (4)	Lao-2	Sand	491	–	2216	23.21	120.8	3.09	14.75	46	15.29	4.63	1.12	0.94	3.88	16.35	0.03	0.06
	Lao-3	Sand	132	–	1630	23.11	120.69	3.92	13.49	55	23.05	3.98	0.79	0.94	2.63	11.14	0.02	0.05
Eastern side																		
Heping (5)	He-1A	Sand	532	506	1469	24.33	121.72	2.21	22.42	22	5.93	2.54	0.99	0.95	2.43	10.41	0.02	0.05
	He-1B	Pebbles	532	506	1469	24.33	121.72	1.7	23	21	3.56	–	–	–	–	–	–	–
Liwu (6)	Li-1	Sand	183	–	1894	24.18	121.49	2.36	18.15	32	8.21	1.76	0.58	0.95	3.2	13.66	0.03	0.06
	Li-2	Sand	433	406	2030	24.18	121.49	3.02	13.61	54	15.97	2.7	0.63	0.94	3.47	14.74	0.03	0.06
	Li-3	Sand	249	223	2144	24.18	121.49	2.9	17.41	35	11.74	12.14	3.37	0.94	3.69	15.63	0.03	0.06
	Li-4	Sand	61	27	1320	24.17	121.6	2.99	14.44	48	14.83	3.87	0.95	0.91	2.09	8.52	0.02	0.05
	Li-5A	Sand	497	–	1814	24.16	121.61	7.25	52.1	4	2.37	–	–	–	–	–	–	–
	Li-5B	Pebbles	497	–	1814	24.16	121.61	1.64	22.4	20	3.35	–	–	–	–	–	–	–
Mugua (7)	Mu-1	Sand	97	56	1890	23.97	121.46	2.64	18.42	32	9.64	3.36	1.03	0.96	3.17	13.65	0.03	0.06
	Mu-2A	Sand	414	286	2023	23.96	121.49	2.61	17.15	34	10.22	2.48	0.73	0.95	3.48	14.86	0.03	0.06
	Mu-2B	Pebbles	414	286	2023	23.96	121.49	2.98	14.96	46	14.29	1.85	0.46	0.95	3.48	14.86	0.03	0.06
Hsinwulu (8)	Hwl-1	Sand	612	586	1910	23.14	121.12	2.37	34.9	9	3.62	–	–	–	–	–	–	–
	Hwl-2	Sand	59	44	1707	23.14	121.12	4.29	14.59	47	23.07	3.83	0.77	0.96	2.69	11.57	0.02	0.05
	Hwl-3	Sand	553	542	1956	23.14	121.12	3.07	14.9	47	14.95	2.14	0.52	0.95	3.27	13.96	0.03	0.06
	Hwl-4	Sand	553	542	1956	23.14	121.12	1.86	20.78	25	4.66	1.29	0.56	0.95	3.27	13.97	0.03	0.06
	Hwl-5	Sand	254	252	2012	23.14	121.11	2.21	18.96	29	7.01	1.67	0.59	0.95	3.41	14.55	0.03	0.06
	Hwl-0808	Sand	254	252	2012	23.14	121.11	2.89	16.91	35	12.06	2.16	0.59	0.95	3.41	14.55	0.03	0.06
	Hwl-6	Sand	298.6	288	1887			3.64	18.66	33	14.07	2.67	0.69	0.95	3.27	13.97	0.03	0.06
Luyeh (9)	Lu0808 a	Sand	469	457	1566	22.9	121.08	5.5	10.98	83	42.46	3.7	0.55	0.95	2.46	10.54	0.02	0.05
	Lu0808 b	Pebbles	469	457	1566	22.9	121.08	3.69	17.95	36	15.06	2.83	0.71	0.95	2.46	10.54	0.02	0.05
	Lu0808 c	Sand	432	420	1629	22.87	121.04	3.86	14.59	47	20.61	2.73	0.58	0.95	2.55	10.91	0.02	0.05
Process Blanks	TWBK7							0.57	70.94	2								

[a] Basin boundaries and areas have been extracted from a digital elevation model (with a resolution of 40 m per pixel) using the Rivertools™ software. Masked areas have been determined according to Chen et al. (2000).

[b] Beryllium-10 data are calibrated directly versus the National Institute of Standards and Technology standard reference material NIST SRM 4325 using an assigned $^{10}Be/^{9}Be$ value of $(2.79 \pm 0.03) \times 10^{-11}$ (Nishiizumi et al., 2007) and a ^{10}Be half-life of $(1.387 \pm 0.012) \times 106$ yr (Korschinek et al., 2010; Chmeleff et al., 2010). Isotopic ratio uncertainties include statistical error on counted ^{10}Be events (N) and analytical error correction.

[c] To assess whether the denudation rates derived from the measured in situ-produced ^{10}Be concentrations are reliable or not, the $^{10}Be/^{9}Be$ isotopic ratios measured within the samples have been compared to that of the companion blank sample (TWBK-7) using the statistical chi-square approach described by Ward and Wilson (1978). The chi-square threshold at 95% confidence for one degree of freedom (2 samples) is 3.84 (see text).

[d] Uncertainties on ^{10}Be concentrations are calculated using the standard error propagation method using the quadratic sum of the relative errors associated to the counting statistics, AMS internal error (0.5% for ASTER), and error associated to the process blank.

[e] To determine basin averaged production rates, scaling factors for latitude and altitude corrections were calculated according to Stone (2000), for each cell of the digital elevation model using the Cronus-Earth Matlab scripts (http://hess.ess.washington.edu/math/). Geomorphic shielding factors were also calculated for each cell of the 40-m resolution digital topography data using a 15° azimuth step following Dunne et al. (1999).

[f] Averaged ^{10}Be production rates (equal to sum of mean production rates for each particle) have been calculated, using a modern ^{10}Be production rate at sea level and high latitude of 4.5 ± 0.3 atoms/g-$_{SiO2}$/yr to account for the reevaluation of absolute calibration of ^{10}Be AMS standards proposed by Nishiizumi et al. (2007) scaling the basin averaged neutron production rate for altitudinal and latitudinal variability (e.g., Stone, 2000), whereas the basin averaged slow and fast muon production rates have been scaled for altitudinal variability only (see Braucher et al., 2011 for discussion).

The equation used to determine the denudation rates sums the exponential equations related to the cosmic secondary particles that are neutrons, slow and fast muons (Braucher et al., 2011):

$$N(x,\varepsilon,t) = \frac{P_{sp}\cdot\exp(-x/L_n)(1-\exp(-t(\varepsilon/L_{sp}+\lambda))}{\frac{\varepsilon\cdot\rho}{L_{sp}}+\lambda} + \frac{P_{\mu s}\cdot\exp(-x/L_{\mu s})(1-\exp(-t(\varepsilon/L_{\mu s}+\lambda))}{\frac{\varepsilon\cdot\rho}{L_{\mu p}}+\lambda} + \frac{P_{\mu f}\cdot\exp(-x/L_{\mu f})(1-\exp(-t(\varepsilon/L_{\mu f}+\lambda))}{\frac{\varepsilon\cdot\rho}{L_{\mu f}}+\lambda} \quad (1)$$

where $N(x,\varepsilon,t)$ is the nuclide concentration as a function of depth (g/cm^2), denudation rate ε (g/cm^2/yr) and exposure time t (yr). P_{sp} is the basin averaged spallation production rate, scaled for altitudinal and latitudinal variability (e.g., Stone, 2000), whereas $P_{\mu s}$ and $P_{\mu f}$ the basin averaged slow and fast muon production rates, scaled for altitudinal variability only (see Braucher et al., 2011 for discussion). The attenuation lengths of neutrons (L_{sp}), slow muons ($L_{\mu slow}$) and fast muons ($L_{\mu fast}$) adopted in this paper are 160, 1500 and 4320 g/cm^2, respectively (Braucher et al., 2011), and λ is the radioactive decay constant of ^{10}Be. Neutrons are very interactive particles and thus not very penetrative compared to negative and fast muons. To account for the density variability through the regolith column exposed to cosmic rays on the hillslopes of the watersheds, we allowed this parameter to vary between 1.8 g/cm^3 (soil) and 2.4 g/cm^3 (rock).

3. Data analysis

3.1. Reliability of the measured isotopic ratios

To ensure that the denudation rates derived from the measured in situ-produced ^{10}Be concentrations are reliable, the ^{10}Be/^{9}Be isotopic ratios measured within the samples have been compared to that of the companion process blank using the statistical chi-square approach described by Ward and Wilson (1978). Taking into account the uncertainties associated with AMS measurements (Table 1), this allows determining if the isotopic ratios measured in the samples are significantly different (from a statistical point of view) from that determined for the process blank. For river samples in Taiwan, this comparison is crucial because the measured isotopic ratios are particularly low (on the order of 10^{-14} to 10^{-15}). The chi-square threshold at 95% confidence for one degree of freedom (2 samples) is 3.8 (Table 1). If the chi-square test value is higher than this threshold, then the isotopic ratio measured in the sample is significantly different from that of the blank process. In that case, a reliable in situ-produced ^{10}Be concentration can be obtained and a denudation rate can be derived from Eq. (1) (Table 2). If the chi-square test value is lower than the chi-square threshold, then the isotopic ratio measured in the sample is not significantly different from that of the blank process within the associated uncertainties, and the sample should be discarded. Among the samples analyzed for this study, only five did not pass this test, strengthening our confidence in the significance of the denudation rates presented here (Table 2).

Once ensured that individual cosmogenic-derived denudation rates are significant from a statistical point of view, we need to address the potential effects of landslides on the ^{10}Be-derived denudation rates. Triggered by typhoons and/or earthquakes, landslides may deliver sediment in the watersheds that was previously buried on the hillslopes deep enough to yield "blank" cosmogenic concentrations. Actually, this situation might bias the cosmogenic signal if samples are taken from immediate downstream of a landslide area; we have therefore avoided these areas. The smaller the sampled watershed is, the more its cosmogenic signal can be influenced by such stochastic inputs of previously buried sediment. This is why, following the recommendations published by Niemi et al. (2005), we concentrated on the larger watersheds to dilute of the landslide effect in the cosmogenic signal.

At cosmogenic steady-state, the cosmogenic ^{10}Be in river-borne quartz mineral record a time integrated, spatially averaged denudation rates which represents fluvially mixed denudation products of all the processes occurring in a given watershed (Bierman and Steig, 1996; Granger et al., 1996). This integration occurs over the time needed to remove one attenuation length (e.g., roughly 60 cm; Lal, 1991). This integration time depends on the denudation rates and is typically on the order of several centuries in Taiwan (Table 2). Such long time scales relative to the high-frequency events (typhoons and earthquakes) allows integrating the hillslope cosmogenic signal, which makes the cosmogenic-derived denudation rates insensitive to short-term stochastic events that dominate sediment flux over several years to decades (Kirchner et al., 2001; Siame et al., 2011). Within this general context, it cannot however be excluded that part of the variability observed between the samples from a given watershed is due to the stochastic effect of mass-wasting events. Nevertheless, the combination of sampling and statistical strategies discussed below ensures a reasonable cosmogenic signal and relevant denudation rates with respect to their magnitudes and regional patterns.

3.2. Identification of outliers and weighted mean values

Outliers, defined as values very different from the majority of cases in a population, are important to identify since they can significantly change the data analysis results. To recognize outliers, we applied the reduced chi-square statistic (e.g., Ward and Wilson, 1978) and determined the mean square weighted deviation (MSWD) for each watershed (Table 3). The MSWD is a measure of over-dispersion, or goodness of fit, that takes into account the relative importance of both the internal and external reproducibility. In other words, the MSWD allows comparing the observed variability within the data population to the expected variability defined by the uncertainties associated to the data (McIntyre et al., 1966). A MSWD value of 1 indicates that the data population fit a univariate normal distribution. The MSWD value is lower than 1 when the observed scatter is less than that predicted by the analytical uncertainties, indicating either overestimated analytical errors or unrecognized error-correlations. The MSWD value is higher than 1 when the observed scatter exceeds that predicted by the analytical uncertainties, indicating either underestimated analytical errors, or the presence of non-analytical scatter (i.e., geological scatter). The actual MSWD value for which the data scatter can be regarded as due to internal reproducibility alone is not limited to the unity but actually varies with the number of data (Wendt and Carl, 1991). For example, to be 95% confident that the scatter of the data is due to the analysis when the number of measurements is equal to 5, an acceptable MSWD range would be 0.2–2.2 (Wendt and Carl, 1991). The numerical results of the MSWD analysis are detailed in Appendix A.

On the western side, the three samples from the Tajia watershed are in good statistical agreement as shown by the unimodal shape of their associated cumulative probability density curve (Fig. 2). All together, the three samples yield a weighted mean of 1.5 ± 0.3 mm/yr with an acceptable MSWD value of 0.53 (Appendix A). For the Wu watershed, the samples Wu-4 and Wu-5 show denudation values that are significantly too low and too high, respectively, when compared to the rest of the population, as illustrated by a bimodal cumulative probability density curve skewed towards high values of denudation (Fig. 2). Rejecting these two samples gives a weighted mean of 0.8 ± 0.1 mm/yr with an acceptable MSWD value of 0.39 (Appendix A). Similarly, for the

Choshui watershed, the cumulative probability density curve is skewed toward high values because of the sample Cho-3A that might also be regarded as an outlier (Fig. 2). Rejecting this particular sample lets the MSWD falling from 2.74 to an acceptable value of 1.91 associated with a weighted mean of 1.5 ± 0.2 mm/yr (Appendix A).

On the eastern side, the Liwu watershed is the catchment where the data are more scattered, as shown by their associated bimodal cumulative probability density curve, which is skewed towards high values of denudation (Fig. 3). Actually, the four samples in the population can apparently be separated into two pairs of samples with the highest (Li-1 and Li-2) and lowest (Li-3 and Li-4) values (Table 2), yielding weighted means of 4.8 ± 1.1 mm/yr and 1.3 ± 0.3 mm/yr, respectively (Appendix A). Within the Hsinwulu watershed, the scattering of the data is also relatively important as illustrated by their associated bimodal cumulative probability density curve, which is also skewed towards high values (Fig. 3). In this case, rejecting the lowest value in the distribution (Hwl-2) yields a relatively well-constrained weighted mean of 5.2 ± 0.8 mm/yr, resulting in an acceptable MSWD value of 0.46 (Appendix A). For the Laonong, Mugua and Luyeh watersheds, only two samples have been collected along the main trunk of each of the rivers (Fig. 1). Given the uncertainties associated to the denudation rates, the pairs of samples are in good agreement with weighted mean values of 2.5 ± 0.5 mm/yr for the Laonong River, 3.8 ± 0.9 mm/yr for the Mugua River, and 2.6 ± 0.4 mm/yr for the Luyeh River (Appendix A). The Heping watershed has only one sample, which yielded a denudation value of 3.4 ± 1.4 mm/yr (Table 2).

3.3. Intra-watershed variability

Although the outlier identification proposed above is solely statistical with the most deviant values being rejected, it appears that rejection of those samples as outliers is also in good agreement with geomorphic considerations. For example, within the Wu watershed, sample Wu-4 was taken at the outlet of the Puli Basin where several levels of Quaternary fluvial terraces have been deposited. River-borne sands sampled at the outlet of the Wu catchment are thus likely to have been contaminated by quartz grains bearing higher ^{10}Be concentrations as a result of their storage in the alluvial terrace deposits. This is supported by the fact that the ^{10}Be concentration measured within sample Wu-4 is more than twice that determined within the sample Wu-6, which was collected upstream of the Puli basin (Fig. 3). In addition, for both the Choshui and Wu watersheds, rejected samples Cho-3A and Wu-5 yielded lower ^{10}Be concentrations and thus higher denudation values with respect to the rest of the samples in their respective population, which is in good agreement with their upstream positions in the watershed closer to the Central Range where exhumation processes should be stronger.

The watersheds draining the western side of the Central Range are particularly influenced by human activity. Since the Taiwanese population is concentrated in the Western Foothills and the Coastal Plain of the island, its vulnerability to natural hazards such as flooding or mass wasting and the use of water for public supply, power generation or irrigation, has resulted in the construction of large water reservoirs on this side of the mountain range (Water Resources Agency, 2012). The western watersheds are also characterized by numerous agricultural facilities along most of their tributaries as well as a large number of quarries excavating sediment and gravel from the riverbeds. However, except for the Wu River catchment, which drains the area around the Puli basin, all the western watersheds exhibit cosmogenic-derived denudation rates that are very similar to ≈2 mm/yr, the value determined for the Lanyang River (Fig. 1), which is in an area less affected by human activity (Siame et al., 2011). Similar denudation rates determined above and below specific reservoirs also suggest little influence of human activity. For example, a comparison of the denudation rates determined from samples collected upstream (1.3 ± 0.4 mm/yr) and downstream (1.8 ± 0.4 mm/yr) of the Deji reservoir in the upper-middle reach of the Tajia River shows that they are not significantly different (Fig. 2). Such observations confirm previous studies performed in similar environmental contexts demonstrating that cosmogenic-derived denudation rates integrated over a 10^2–10^3 yr-time scales are not impacted by recent human activity but rather reflect a natural background denudation value (Brown et al., 1998; Hewawasam et al., 2003).

The variability observed in the Liwu watershed is strongly linked to the anomalously low value determined for the sample Li-3. Indeed, samples Li-1 and Li-3 correspond to the main sub-basins draining the headwaters of the catchment, whereas sample Li-2 has been collected within the major trunk of the Liwu River just downstream of the confluence between Li-1 and Li-3 sub-basins (Fig. 3). Li-4 is a small tributary catchment close to the outlet of the Liwu River (Fig. 3). Given the denudation values derived for Li-1 and Li-2, one would expect the denudation rate derived from Li-3 to be on the same order of magnitude. Why the rate of this particular sample is much lower respect to its neighbors remains an open question since the sampling protocol is the same as for the other samples. Among the four samples, Li-2 appears to be the more representative for the Liwu catchment since it corresponds to a catchment that encompass both Li-1 and Li-3 sub-basins (Fig. 3). However, given the relatively large errors associated to the denudation values determined for the Liwu watershed, a rather conservative assumption would be to consider that the denudation ranges from 1.3 ± 0.3 to 4.8 ± 1.1 mm/yr.

3.4. Bootstrap analysis

In the previous sections, we discussed the presence of outliers and thus proposed weighted means for the denudation rates within each studied watersheds. The mean square weighted deviation approach assumes that the denudation rates have normal and independent uncertainties. If all the associated errors were to be randomly distributed, the cumulative probability density curves derived from the data sets should have a symmetrical, Poisson-like distribution. However, most of the cumulative probability density curves derived for the sample populations are skewed and/or bimodal in shape (Figs. 2 and 3). To downplay the weight of high outliers, we applied a non-parametric bootstrap technique, which allows estimating statistical parameters such as the mean and the median together with their associated standard deviations.

Bootstrapping is a computer-based statistical method that is particularly useful for small data sets and/or when probability distributions are non-normal (Efron, 1979; Efron and Tibshirani, 1986, 1993; Davison and Hinkley, 1997). Based on resampling with replacement, this technique assumes that the set of observations is an adequate model for the studied population and that resampling over that observation set on a large enough scale will reveal the population distribution characteristics. For each watershed, data sets of n samples $\{x_1,\ldots,x_n\}$ were produced using the minimum and maximum denudation rate values in order to account for all sources of uncertainties. For each data set, B (B = 15,000) bootstrap replicates $\{x_1^*,\ldots,x_n^*\}$, where x_i^* is a random value with replacement from $\{x_1,\ldots,x_n\}$, were obtained without any distributional assumption. Finally, for each bootstrap replicate mean and median values were calculated and the distribution of these B estimates represents the bootstrap estimates of uncertainty about the true values of the considered statistic parameters (Table 3). Accounting for the standard deviations associated to the weighted mean values, assuming that denudation rates have normal and

Table 2
Drainage basin metrics, denudation rates and integration times as determined for the studied watersheds.

Watershed	Sample ID	Centroïd[a]		Distance[b] (km)	Strahler order	Area (km^2)	Relief (m)	Hypsometric index	Elevation (m)			Mean	Denudation (mm/yr)		Integration time (yr)	
		Lon. (°E)	Lat. (°N)						Min	Max	Mean	Slope (°)	Value	Error	Value	Error
Lanyangchi	Siame et al. (2011)	121.4	24.5	288	7	364	3241	0.35	280	3521	1423	30.4	2.0	1.0	381	190
Western side																
Tajia (1)	Ta-1	121.2	24.3	253	7	964	3417	0.48	465	3882	2093	32.9	1.8	0.4	414	96
	Ta-3A	121.3	24.4	268	6	155	2356	0.39	1526	3882	2436	33.0	1.4	0.5	558	187
	Ta-3B	121.3	24.4	268	6	155	2356	0.39	1526	3882	2436	33.0	4.9	1.4	156	43
	Ta-4A	121.3	24.3	263	7	418	2450	0.41	1432	3882	2444	31.8	1.3	0.4	601	193
	Ta-4B	121.3	24.3	263	7	418	2450	0.41	1432	3882	2444	31.8	6.1	1.6	126	32
Wu (2)	Wu-1	121.0	24.1	223	8	996	3211	0.28	181	3392	1073	26.5	0.7	0.2	1029	224
	Wu-2	120.9	24.1	224	6	78	1259	0.35	269	1528	716	23.2	0.9	0.2	832	177
	Wu-3	121.1	24.1	233	6	435	3128	0.38	264	3392	1464	32.2	1.0	0.3	745	188
	Wu-4	121.0	24.0	214	8	420	2173	0.27	246	2419	823	22.1	0.2	0.0	3378	566
	Wu-5	121.1	24.1	237	6	337	2958	0.42	434	3392	1677	33.9	1.8	0.4	417	100
	Wu-6	121.1	24.0	224	6	98	1887	0.39	532	2419	1264	31.4	0.8	0.2	1006	296
Choshui (3)	Cho-1	121.0	23.7	191	8	2892	3770	0.39	86	3856	1555	29.3	2.3	0.5	336	80
	Cho-2	121.0	23.8	196	8	2196	3735	0.44	121	3856	1783	31.6	1.8	0.4	435	93
	Cho-3A	121.1	23.8	203	8	1486	3362	0.46	442	3804	1997	32.6	3.8	1.1	203	58
	Cho-3B	121.1	23.8	203	8	1486	3362	0.46	442	3804	1997	32.6	10.0	3.3	76	25
	Cho-4	121.1	23.8	203	8	1537	3440	0.47	364	3804	1975	32.7	1.2	0.2	621	115
Laonong (4)	Lao-2	120.9	23.3	146	7	491	3318	0.48	623	3941	2217	34.3	2.8	0.8	270	77
	Lao-3	120.8	23.1	121	6	132	2867	0.44	376	3243	1632	32.8	2.3	0.6	330	83
Eastern side																
Heping (5)	He-1A	121.6	24.4	282	7	532	3591	0.39	43	3634	1455	32.2	3.4	1.4	224	94
Liwu (6)	Li-1	121.5	24.3	266	6	183	3279	0.45	429	3708	1894	33.3	6.3	2.3	121	44
	Li-2	121.4	24.2	258	7	433	3292	0.49	416	3708	2014	34.3	4.4	1.2	173	49
	Li-3	121.4	24.2	253	6	249	3133	0.53	434	3567	2106	35.1	1.0	0.3	738	234
	Li-4	121.6	24.2	268	5	61	2565	0.48	84	2649	1312	37.7	1.9	0.5	410	119
Mugua (7)	Mu-1	121.4	24.0	231	5	97	3123	0.49	214	3337	1739	33.2	3.3	1.1	231	79
	Mu-2A	121.4	24.0	237	7	414	3467	0.50	130	3597	1851	34.0	4.8	1.6	158	53
	Mu-2B	121.4	24.0	237	7	414	3467	0.50	130	3597	1851	34.0	6.5	1.9	118	35
Hsinwulu (8)	Hwl-2	121.1	23.2	142	5	59	2630	0.48	375	3005	1625	31.7	2.5	0.6	306	77
	Hwl-3	121.0	23.2	133	7	553	3300	0.48	362	3662	1940	31.7	5.3	1.5	144	42
	Hwl-4	121.0	23.2	133	7	553	3297	0.48	365	3662	1940	31.7	8.8	4.0	87	40
	Hwl-5	121.0	23.2	139	6	254	3275	0.49	387	3662	2006	32.3	7.0	2.7	108	42
	Hwl-0808	121.0	23.2	139	6	254	3275	0.49	387	3662	2006	32.3	5.4	1.7	140	44
	Hwl-6	121.0	23.1	128	6	299	2905	0.52	375	3280	1886	31.2	4.1	1.2	186	56
Luyeh (9)	Lu0808 a	120.9	22.9	107	7	469	3070	0.46	151	3221	1565	31.3	2.4	0.5	322	69
	Lu0808 b	120.9	22.9	107	7	469	3070	0.46	151	3221	1565	31.3	3.1	0.9	246	72
	Lu0808 c	120.93	22.92	106	7	432	2993	0.47	228	3221	1628	31.6	3.3	0.9	230	60

Basin metrics have been extracted from a digital elevation model (with a resolution of 40 m per pixel) using the Rivertools™ software. (c) Averaged basin-wide denudation rates (mm/yr) have been calculated using Eq. (1) (e.g., Braucher et al., 2011), the parameters given in Table 1 and those described in the text. Uncertainties include ^{10}Be concentration error (Table 1), 6% error on production rate (e.g., Stone, 2000) and 14% error on density (for the exposed material to cosmic rays. we assumed a density of 2.1 ± 0.3 g/cm^3). (d) Integration times are calculated after Lal (1991) and their uncertainties are calculated propagating those of the denudation rates.

[a] Watershed centroids have been determined as the center of gravity using the basin boundaries.

[b] Horizontal distances of the watershed centroids with respect to the southern tip of the Hengchun Peninsula have been determined using the Geographical Information System Mapinfo™.

independent uncertainties, and those estimated for the bootstrap mean and median values, determined without any distributional assumption, all the estimators for the central tendency are in good agreement (Table 3 and Fig. 4). However, unlike the mean, the median is an estimate for the central tendency that offers the advantage of being insensitive to extreme values and skewed distributions. In addition, for cosmogenic-derived denudation rates determined from river-borne sands sampled in landslide-dominated catchments, Niemi et al. (2005) showed that the median value is more representative for the volumetric erosion rates. Given these reasons and taking into account that bootstrap estimators are statistically law-independent, we decided to use the bootstrap median values and their associated standard deviations for further discussion of the orogen-scale denudation (see Section 4). The bootstrap-derived mean and median values determined for each watershed are presented in form of histogram density plots (Figs. 2 and 3) and in Table 3.

3.5. Comparison between amalgamated pebbles and sand samples

For some of the studied watersheds, samples of quartz pebbles were also collected in the same area as the sand samples. For the samples of pebbles that passed the chi-square test against the blank process (Table 1), we compared the in situ-produced ^{10}Be concentrations measured within the companion pebble and sand samples (Appendix A). Except for the pairs Mu-2A/Mu-2B and Lu0808a/Lu0808b where the ^{10}Be concentrations are not statistically different, the ^{10}Be concentrations measured in the amalgamated pebbles are roughly 3–5 times lower than those measured in the sand samples (Table 1). This is the opposite observation than that made by Codilean et al. (2014) in the desert setting of Namibia. Although more samples would be necessary to delineate with higher confidence a general trend, a preliminary interpretation is that amalgamated pebbles are not properly mixed within the regolith and thus may not properly spatially integrate the watershed.

Table 3
Summary of the denudation rate central values determined for the studied watersheds.

Watershed	Statistic				Bootstrap			
	Weighted mean		Mean		Mean		Median	
	Value	1σ	Value	1σ	Value	1σ	Value	1σ
Tajia	1.49	0.25	1.49	0.55	1.49	0.21	1.48	0.31
Wu	0.83	0.10	0.86	0.26	0.86	0.09	0.84	0.12
Choshui	1.48	0.18	1.75	0.64	1.75	0.24	1.67	0.30
Laonong	2.48	0.47	2.57	0.87	2.56	0.37	2.52	0.52
Western side	1.63	0.13	1.85	0.73	1.86	0.17	1.75	0.19
Liwu	–	–	–	–	3.91	1.09	3.63	1.45
Mugua	3.80	0.92	4.07	1.83	4.07	0.79	3.97	1.06
Hsinwulu	5.20	0.80	5.52	3.17	5.52	0.87	4.71	0.95
Luyeh	2.61	0.44	2.85	0.99	2.85	0.43	2.78	0.56
Eastern side	4.21	0.43	4.70	2.63	4.70	0.51	4.07	0.47
				Whole range	3.62	0.39	2.94	0.4

Weighted means have been determined following the statistical chi-square approach described by Ward and Wilson (1978). Bootstrap mean and median values have been computed using XLSTAT™. Values are given in mm/yr.

However, a larger scale comparison would be useful to determine denudation rates for watersheds where the quartz content within the sand fraction is too low to yield satisfactory ^{10}Be concentration measurements. Given the number of samples and the observation that ^{10}Be concentrations in the quartz pebbles are 3–5 times lower than in quartz sands, any derived denudation rates from amalgamated quartz pebbles should be corrected accordingly.

3.6. Basin-wide denudation rates

In north-central Taiwan, the Tajia and the Wu watersheds, both draining to the west from the Hsüehshan and Central ranges, are characterized by denudation rates (bootstrap median values) that are 1.5 ± 0.3 mm/yr and 0.8 ± 0.1 mm/yr, respectively (Fig. 2). At the same latitude, but on the eastern side of the range, the Heping, Liwu and Mugua watersheds show denudation rates of 3.4 ± 1.4 mm/yr, 3.9 ± 1.5 mm/yr, and 4.0 ± 1.0 mm/yr, respectively (Fig. 3). In the case of the Heping catchment, where only one sample was measured, we assume that the determined denudation value is representative for the watershed. For the Liwu watershed, we applied the bootstrap to the range of values determined for the samples Li-1, Li-2, and Li-3, excluding the sample Li-4, which is not representative for the watershed. The bootstrapped mean and median values fall between the lower and upper bounds estimated from the weighted-means discussed above, that is 3.9 ± 1.1 mm/yr and 3.6 ± 1.5 mm/yr, respectively (Table 3). In central and south-central Taiwan, the Choshui and Laonong watersheds show denudation rates (bootstrap median values) of 1.7 ± 0.3 mm/yr and 2.5 ± 0.5 mm/yr, respectively (Fig. 2). At the same latitude but on the eastern side of the range, the Hsinwulu and Luyeh watersheds exhibit significantly higher denudation rates (bootstrap median values) of 4.7 ± 0.9 mm/yr and 2.8 ± 0.6 mm/yr, respectively (Fig. 3).

3.7. Characteristic denudation rates for the Taiwan belt

In this study, all the watersheds encompass the central part of the Taiwan mountain belt, that is the section of the belt where the collision is mature (Fig. 1). On both sides of the range, significant central values can be derived from the cosmogenic-derived denudation rates (Fig. 5). For the western side, the skewed cumulative probability density curve is also significantly influenced by the lowest values from the Wu watershed, which should not be considered as representative for the characteristic denudation rate on this side of the belt. To derive such a characteristic value, the samples from the Wu watershed have thus been excluded with the exception of sample Wu-5, which is located in the upstream headwaters of the Wu catchment. The weighted mean derived from the remaining western samples is 1.6 ± 0.1 mm/yr resulting in a chi-square test value of 13.6 that is lower than the chi-square threshold of 16.9 for 9 degrees of freedom at 95% confidence level (Appendix A). Bootstrapping this data population allows estimating a mean value of 1.9 ± 0.2 mm/yr and a median value of 1.8 ± 0.2 mm/yr (Table 3 and Fig. 5).

For the eastern side of the central part of the Taiwan belt, the cumulative probability density curve is also both influenced by the lowest values in the data population and skewed toward high values of denudation because of the uncertainties associated to the data. However, removing the lowest values from the Liwu, Hsinwulu and Luyeh catchments (Li-4, Hwl-2, and Lu0808a) yields a weighted-mean of 4.2 ± 0.4 mm/yr resulting in a chi-square test value of 6.4 that is lower than the chi-square threshold of 18.3 for 10 degrees of freedom at 95% confidence level (Appendix A). Bootstrapping the same data population allows estimating a mean value of 4.7 ± 0.5 mm/yr and a median value of 4.1 ± 0.5 mm/yr (Table 3 and Fig. 5). Finally, considering both the western and eastern watersheds and bootstrapping the data populations discussed above allows estimating a mean value of 3.6 ± 0.4 mm/yr and a median value of 2.9 ± 0.4 mm/yr (Table 3). This denudation rate, ranging from 2.5 to 4 mm/yr, should be regarded as the characteristic value for the Taiwan Mountains over a centennial time scale.

4. Discussion

The presented data enable us to ask whether or not the pattern of cosmogenic-derived denudation rates reflect the processes supporting the orogeny-scale topography. Indeed, the narrow, steep and highly denudating eastern side of the mountain belt contrasts with the wider and slowly denudating western side, which may likely result from the underlying mechanics, that is accretion along the western front and underplatting at depth below the Central Range (Malavieille, 2010). However, keeping in mind these essential regional-scale topographic inputs, do other observables such as drainage basin metrics (area, relief, and slope) or precipitation patterns significantly impact the cosmogenic-derived denudation rates on centennial time-scales?

4.1. Testing cosmogenic-derived denudation rates against watershed metrics

The lack of relationship between watershed areas and cosmogenic derived denudation rates (Fig. 6a) is an observation already

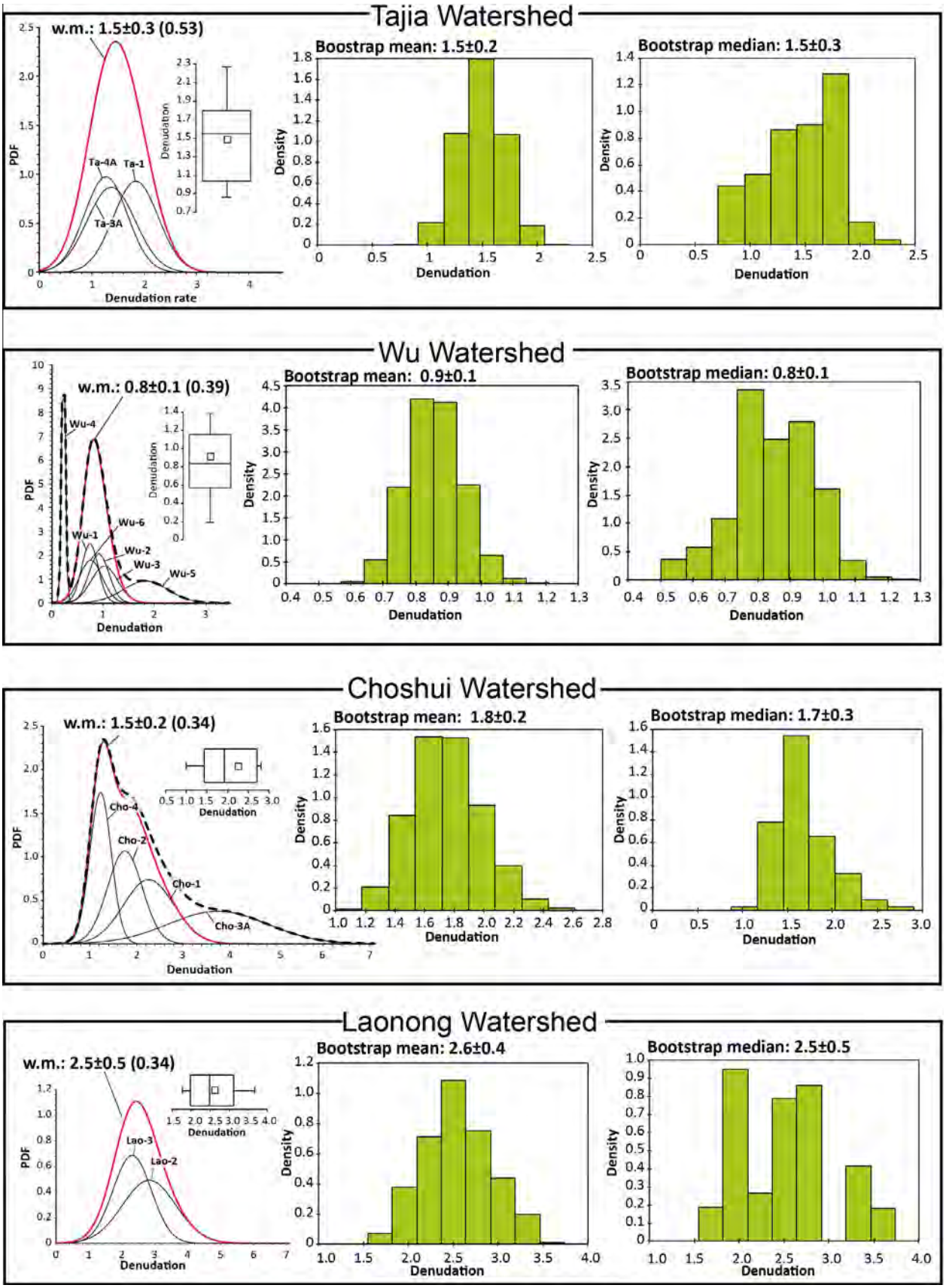

Fig. 2. Cosmogenic-derived denudation rates for the studied western watersheds. Left: Cumulative probability density curves of the samples (black thin lines), of the data population (black dashed line), of the sample population included in the weighted-mean (red thick line) and associated box plot displaying the first quartile, median (horizontal line), mean (open square), and third quartile together with both upper and lower limits (whiskers). w.m., weighted mean with MSWD value in parenthesis. Right: Bar histograms of the bootstrap resampling showing the density (ratio of the frequency to the size of the interval) of the mean and median denudation rates for each watershed. All numbers are given in mm/yr and are reported in Table 3. (For interpretation of the references to color in this figure legend, the reader is referred to the web version of this article.)

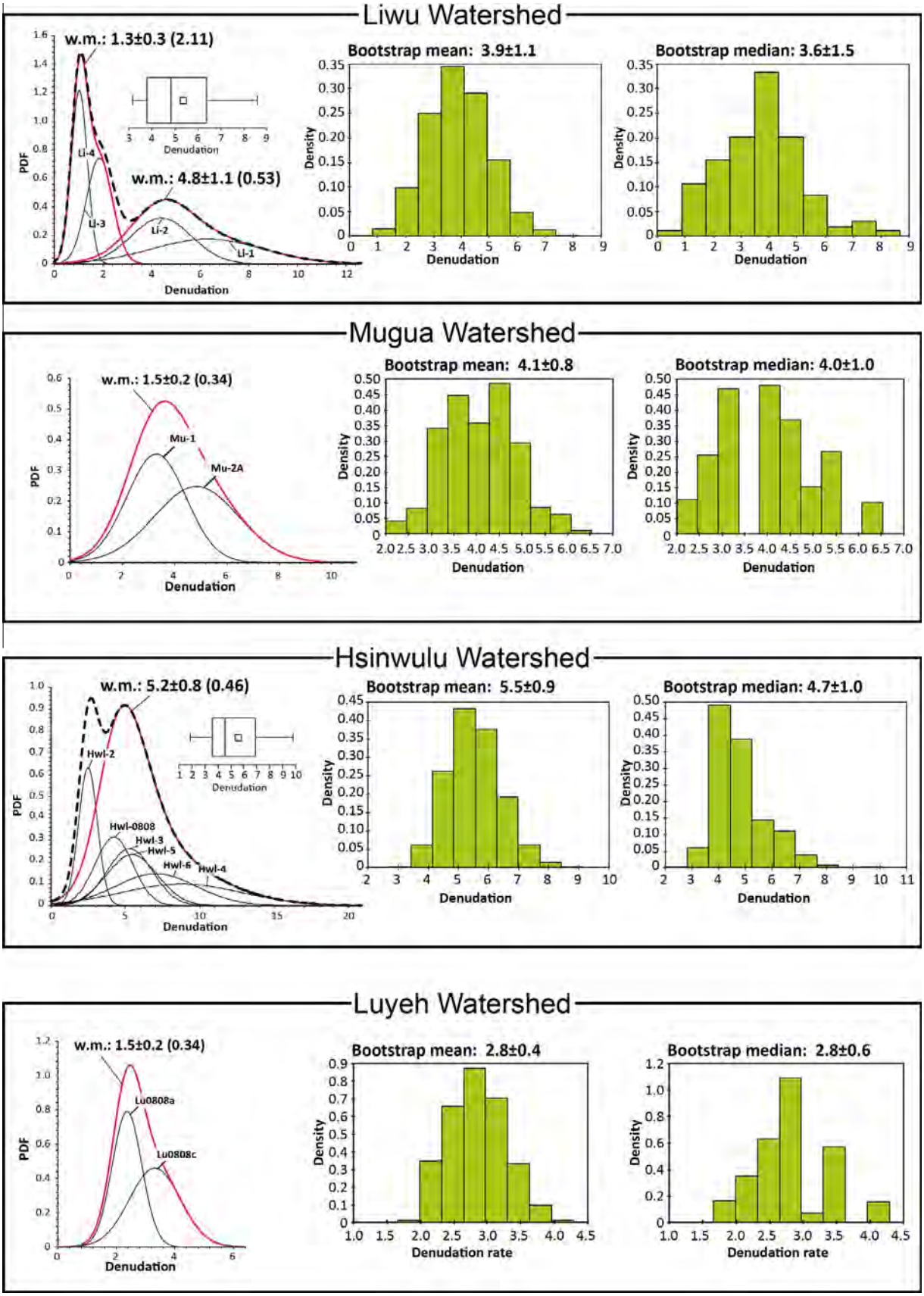

Fig. 3. Cosmogenic-derived denudation rates for the studied eastern watersheds. Left: Cumulative probability density curves of the samples (black thin lines), of the data population (black dashed line), of the sample population included in the weighted-mean (red thick line) and associated box plot displaying the first quartile, median (horizontal line), mean (open square), and third quartile together with both upper and lower limits (whiskers). w.m., weighted mean with MSWD value in parenthesis. Right: Bar histograms of the bootstrap resampling showing the density (ratio of the frequency to the size of the interval) of the mean and median denudation rates for each watershed. All numbers are given in mm/yr and are reported in Table 3. (For interpretation of the references to color in this figure legend, the reader is referred to the web version of this article.)

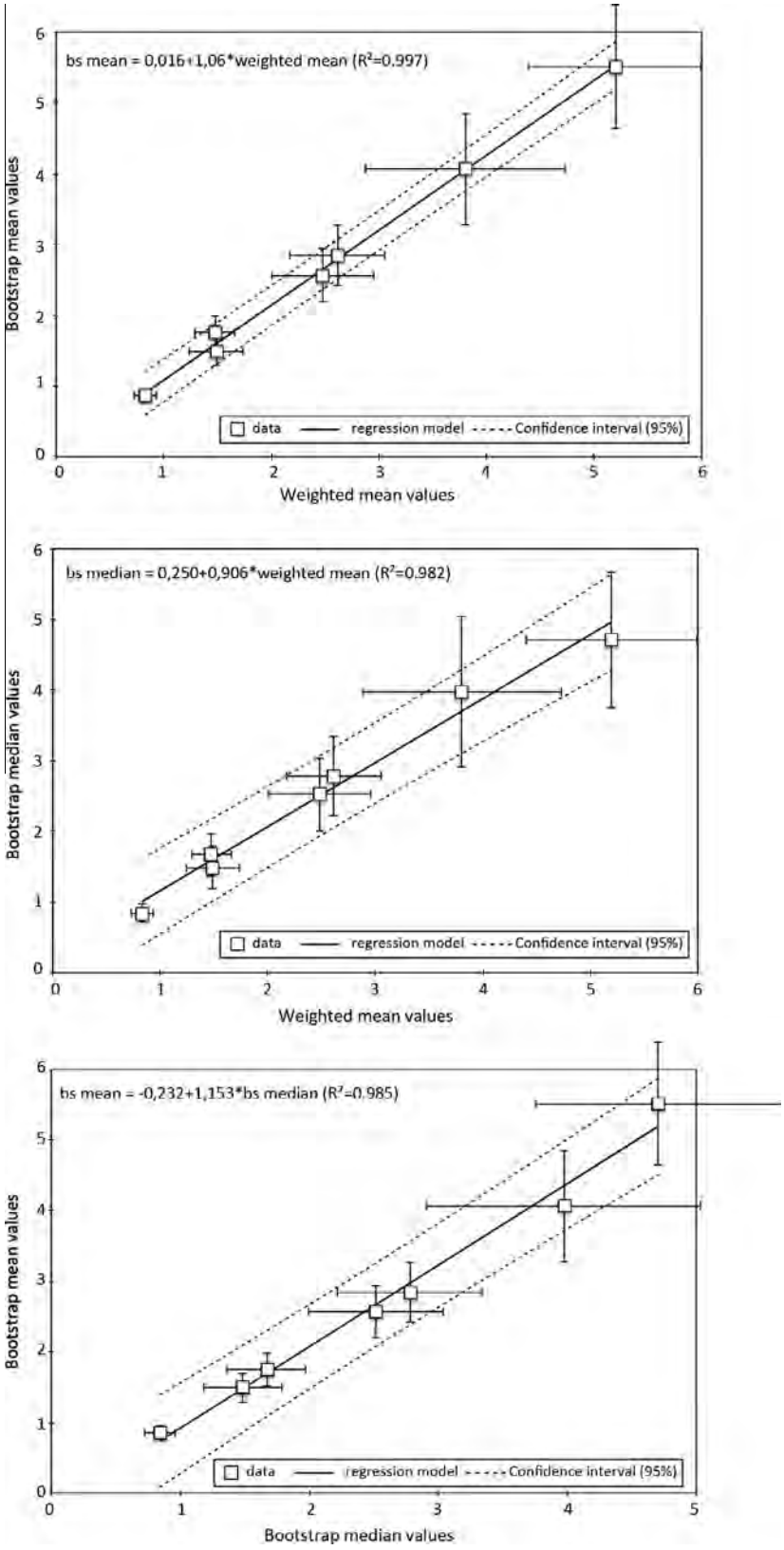

Fig. 4. Comparison between the weighted means, bootstrap mean and bootstrap median values. The values are reported in Table 3.

reported by Portenga and Bierman (2011), using a global data set. In addition, Portenga and Bierman (2011) highlighted this result as important since it reflects that changes in the sediment delivery ratio do not affect estimation of denudation rates from a cosmogenic point of view. In recent local studies, drainage basin denudation rates have been shown to correlate well with average basin elevation (Heimsath et al., 2006; Palumbo et al., 2009). As far as our data set is concerned, this relationship also exists in Taiwan, even though some variability is due to data scattering (Fig. 6b). For example, considering the main drainage basins together with their

respective bootstrap median values of denudation, the bivariate relationship is medium ($r^2 = 0.41$). If the western and eastern watersheds are considered separately, the correlation turns out to be slightly better for western drainage basins ($r^2 = 0.73$) than for the eastern ones ($r^2 = 0.63$).

The hypsometric index (HI), calculated as the ratio of the mean basin incision ($E_{mean} - E_{min}$) to the basin's relief ($E_{max} - E_{min}$), is related to the degree of dissection of a given watershed. This geomorphic index is commonly used to discriminate between tectonically active and inactive regions (Strahler, 1952). Values larger than 0.5 are generally viewed as indicating youthful or rejuvenated topographies, dominated by diffusive hillslope processes, while lower values indicate more mature topographies and watersheds dominated by fluvial processes (Strahler, 1952; Willgoose and Hancock, 1998). For the presented data set, the drainage basins separate into two distinctive groups with the western watersheds having HI values ranging from 0.27 to 0.47 and the eastern watersheds exhibiting HI values ranging from 0.45 to 0.53 (Table 2). Considering the main drainage basins together with their respective bootstrap median values of denudation, the correlation with the HI values is medium ($r^2 = 0.42$). However, for the western side of the belt, this bivariate relationship is much stronger ($r^2 = 0.73$) than for the eastern side ($r^2 = 0.22$). On the eastern side, the poor correlation is due to the relatively low denudation value for the

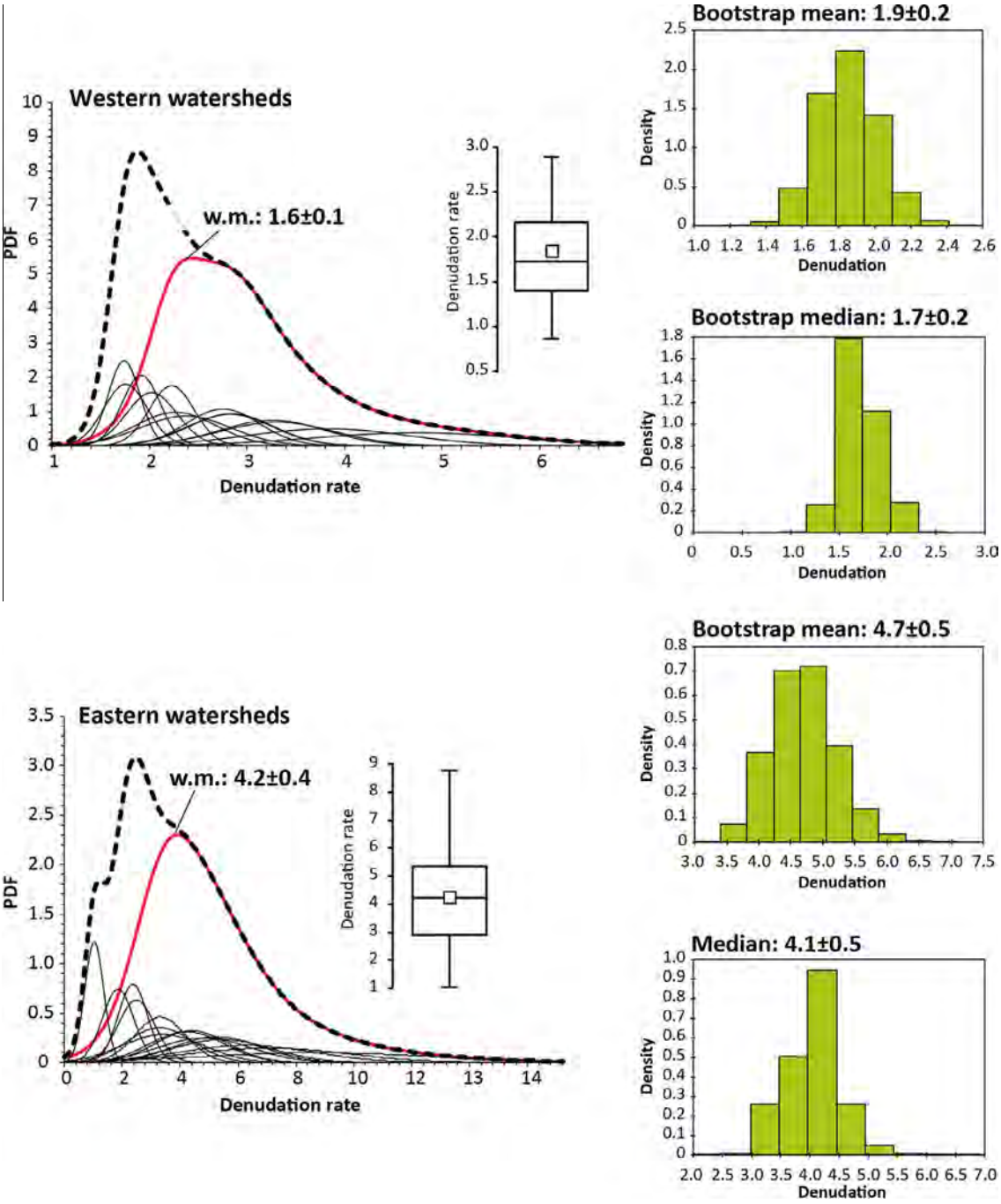

Fig. 5. Cumulative probability density curves (weighted means) and bar histograms of the bootstrap resampling for the western (up) and eastern (down) watersheds (same legends as for Figs. 2 and 3). All numbers are given in mm/yr and are reported in Table 3.

Luyeh watershed given its characteristic HI value (Fig. 6c). If this particular watershed is removed from the relationship, the correlation becomes more significant ($r^2 = 0.73$).

Together with relief, basin slope is also related to drainage basin denudation rates, producing significant bivariate relationships on the global scale (Portenga and Bierman, 2011). For the presented dataset, this relationship is obscured by the data scattering due to the large uncertainties associated to the denudation rates determined for the eastern watersheds. However, considering the main drainage basins, the bivariate relationship between denudation rate (bootstrap) and mean basin slope is medium ($r^2 = 0.41$). For the western side of the belt, the bivariate relationship between denudation and mean basin slope of the drainage basins is more significant ($r^2 = 0.73$) than for the eastern side ($r^2 = 0.22$). On the eastern side the poor correlation is apparently due to the relatively high denudation value for the Hsinwulu watershed given its characteristic mean slope value (Fig. 6d). If this particular watershed is removed from the relationship, the correlation becomes more significant ($r^2 = 0.92$).

From the geomorphic point of view, it thus appears that the observed variance in the denudation rates determined for the central part of the Taiwan Mountains can be, to some extent, associated to relief and slope, which are both linked to the tectonic activity. Indeed, when comparing the basin mean slope with the HI values, it appears that the watersheds with the higher denudation rates are generally those characterized with the higher mean slope and/or HI values (Fig. 6e). However, for the same mean slope or HI range, the western Tajia and Laonong watersheds exhibit denudation rates that are significantly lower than those from the eastern side. One can argue that this contrast in denudation rates between western and eastern watersheds reflects the pattern of strong annual precipitations. Indeed, for the whole island of Taiwan, the average precipitation rate determined for the period between 1949 and 2009 is 2500 mm/yr (Water Resources Agency, 2014). In northern Taiwan, the average precipitation rate is 2930 mm/yr, contrasting with that of the southern-southwestern region (2520 mm/yr). For central Taiwan, the western side of the belt is characterized by an average precipitation rate of 2150 mm/yr, which contrasts the precipitation rate of 2540 mm/yr for the eastern side. However, for the studied watersheds, the average precipitation rate typically ranges from 2500 to 3000 mm/yr with no significant difference between east and west. It thus seems that, at least for a first order analysis, the mean annual precipitation pattern does not explain that of the denudation rates (Fig. 7a). Portenga and Bierman (2011) also made this observation at a more global scale.

4.2. Along-strike cosmogenic-derived denudation pattern

To illustrate the along-strike denudation pattern for the Taiwan mountain belt, we plotted the horizontal distances measured between the southern tip of the belt (Hengchun Peninsula) and the watershed centroids against the denudation rates (bootstrap medians) determined for each watershed (Fig. 7b). For the central segment of the belt, the orogen-scale pattern of denudation is twofold: (1) higher denudation values, on the order of 4–5 mm/yr, characterize the eastern side of the belt (retro-wedge), with a

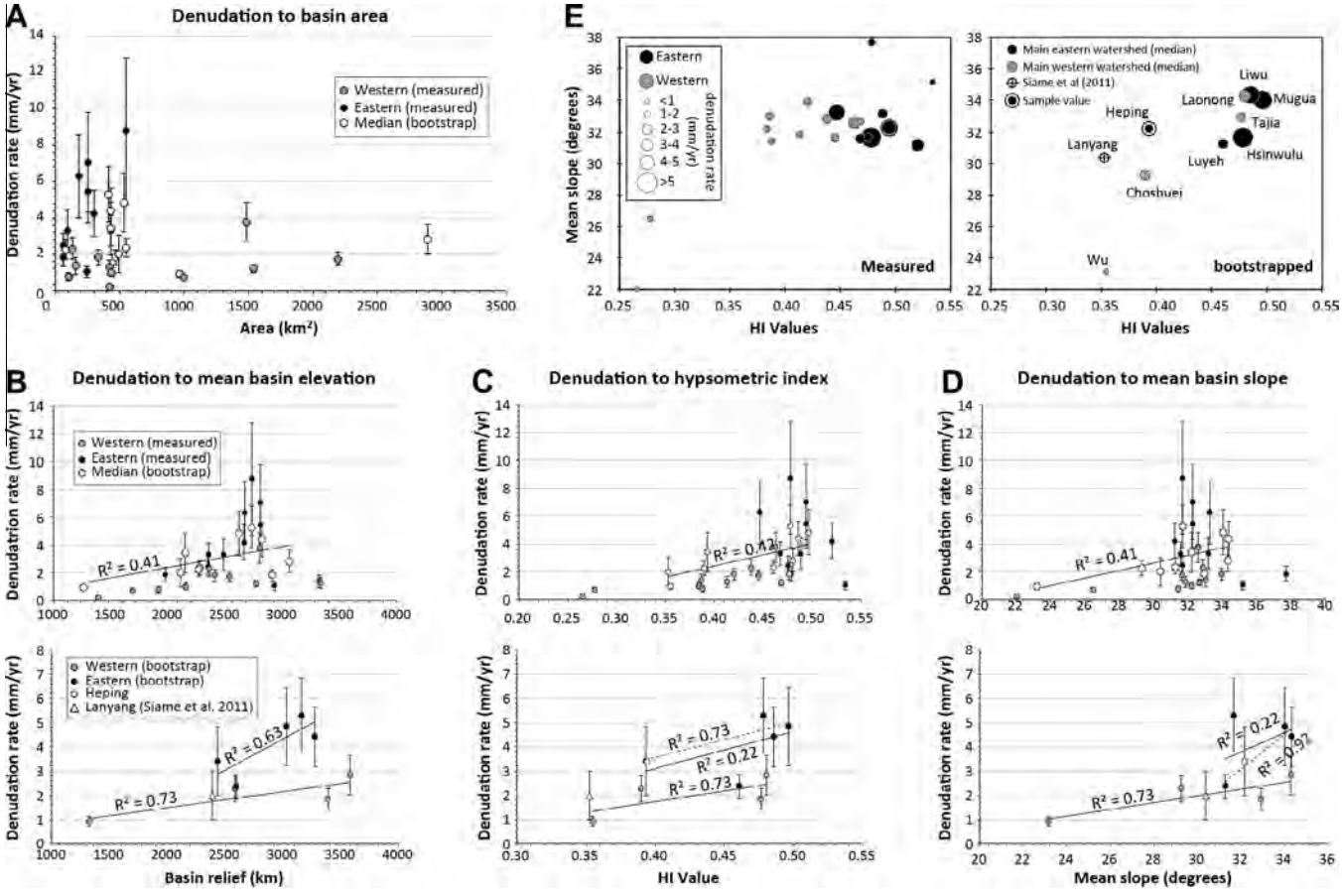

Fig. 6. Cosmogenic-derived denudation rates to basin metrics relationships. (A) Relationship of denudation rates to basin area. (B) Relationship of denudation rates to mean basin elevation. (C) Relationship of denudation rates to hypsometic index calculated as the mean basin incision ($E_{mean} - E_{min}$) divided by the basin relief ($E_{max} - E_{min}$). (D) Relationship of denudation rates to mean basin slope. (E) Relationship of mean basin slope to hypsometric index. The size of the circles is a function of the denudation rate magnitude.

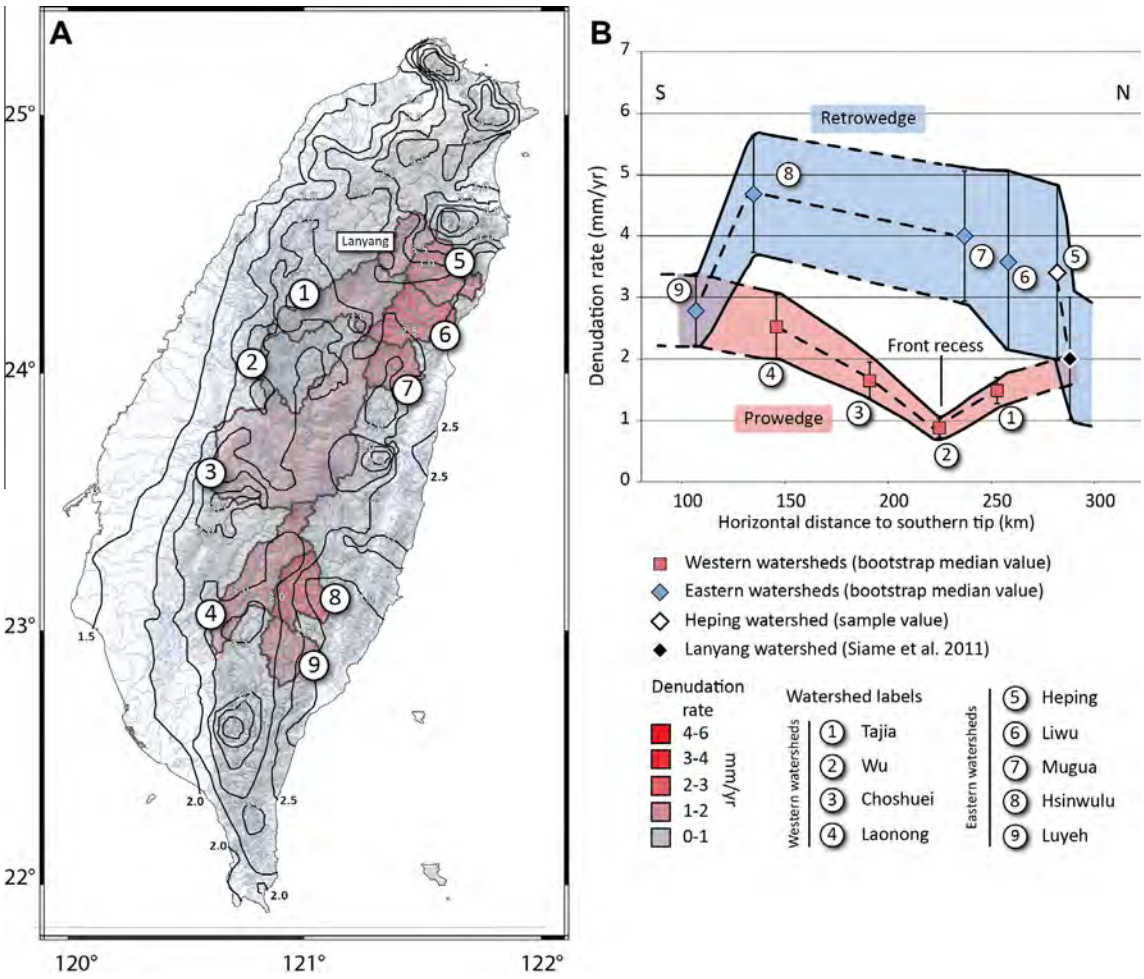

Fig. 7. Denudation pattern of the Taiwan mountain belt as determined from cosmogenic ^{10}Be measurements. Left: Map of Taiwan displaying the studied watersheds with colors as a function of denudation rates (bootstrap median value). Black solid lines (isohyetal contours) indicate distribution of average annual precipitation for the period encompassing 1949–2009 (Water Resources Agency, 2014). Right: Along-strike denudation pattern of the Taiwan mountain belt. Denudation values are plotted as a function of the horizontal distance to southern tip of the belt.

slight increase towards the south; (2) lower denudation values, on the order of 1–3 mm/yr, characterize the western side of the belt (pro-wedge). A second order observation is the low denudation rates determined for the part of the western Central segment corresponding to the Puli basin (Wu watershed). This region of low elevation and low relief lies within the well-developed thrust-and-fold belt, is located above a deep, relatively rigid, crustal promontory (known as the Peikang High in central Taiwan), and corresponds to an orogenic syntaxis that divides the orogen both along and across strike (see Byrne et al., 2011). To the north and to the south of the central segment, the denudation rates converge towards values on the order of 2–3 mm/yr (Fig. 7b).

The centennial cosmogenic-derived denudation rates determined in this study are in good agreement with the long-term rates of denudation derived from low-thermochronology techniques. In the Central Range, published exhumation rates derived from fission-track data show relatively low values, on the order of ≈1 mm/yr, in the west, and higher values, on the order of ≈5 mm/yr, in the east (Liu et al., 2001; Willett et al., 2003). A recent reappraisal using a two-dimensional thermo-mechanical model for the orogeny suggests that current average denudation rates should be slightly lower on the east, on the order of 3 mm/yr, and 2 mm/yr over the whole island to predict the measured apatite and zircon fission track ages (Fuller et al., 2006). These values are within the range of the denudation rate averaged for the mountain belt presented in this study (Table 3). In striking contrast, both the centennial cosmogenic-derived denudation rates and the long-term exhumation rates are systematically lower than the decadal leveling-derived surface uplift rates, on the order of 10–15 mm/yr, that have been determined in the Central Range (Ching et al., 2011). The good agreement between short-term cosmogenic-derived denudation rates and long-term exhumation rates, combined with higher relief, slope and hypsometric index values, as well as outcrops of the highest metamorphic grade in Taiwan, all point to the eastern Central Range being an area of sustained high denudation for the duration of the orogenic event. The deeply eroded and steep catchments located in the eastern part of the mountain belt and the more mature western landscape may thus reflect the different exhumation rates that characterize each side of the Central Range.

5. Conclusions

The Taiwan mountain belt serves as one of the best examples in the world to understand and study mountain building processes. In this study, we quantified centennial rates of denudation at the scale of the whole orogen of Taiwan, using in situ ^{10}Be concentrations measured in stream sediments collected at the outlets of major rivers. For the central segment of the belt, where the collision is

considered to be near mature, the orogen-scale pattern of denudation shows a two-fold pattern with higher denudation values on the order of 4–5 mm/yr characterizing the eastern side of the belt (i.e., retro-wedge), with a slight increase towards the south, and lower denudation values on the order of 1–3 mm/yr on the western side of the belt (pro-wedge) with a minimum value centered on the main recess of the deformation front. To the north and to the south of the central segment, the denudation rates converge towards lower values on the order of 2–3 mm/yr. At the scale of the mountain belt, drainage basin metrics such as relief, hypsometric index and slope values seem to explain the observed variance in the data population, conversely to the first-order average precipitation pattern, suggesting a strong tectonic control on denudation rates within the segment of the belt where the collision is mature. Further investigations using cosmogenic-derived denudation rates are needed towards the south and the north of the mountain belt to decipher the regional pattern of denudation rates in connection with waning and incipient collision. The results presented here are important because they characterize and quantify one of the main processes involved in the evolution of orogenic wedges, denudation. Our results help understanding the evolution of Taiwan – an iconic orogenic system – and provide constraints on input parameters used in analog and numerical models of orogenic systems.

Acknowledgments

The French AMS national facility ASTER (CEREGE, Aix-en-Provence) is supported by the INSU/CNRS, the ANR through the "Projets thématiques d'excellence" program for the "Equipements d'excellence" ASTER-CEREGE action, IRD and CEA. We are grateful to Maurice Arnold, Georges Aumaître and Karim Keddadouche for their invaluable help during the ^{10}Be AMS measurements. We also thank Chu-Chun Kung and Fong-Min Chou for their help during fieldwork. We also acknowledge the BFT (Bureau Français de Taipei) and the BRT (Bureau de Représentation de Taipei en France) for their constant help; CNRS-INSU in France, NSC (National Science Council) in Taiwan and the Office of International Science and Technology and the Tectonics Program in the US National Science Foundation. During 2013 and 2014, Lionel L. Siame has been appointed as Visiting Associate Research Fellow at Institute of Earth Sciences, Academia Sinica of Taiwan (NSC 102-2811-M-001) and benefited from a delegation position at CNRS. This is contribution of the Institute of Earth Sciences, Academia Sinica, IESASxxxx.

Appendix A. Supplementary material

Supplementary data associated with this article can be found, in the online version, at http://dx.doi.org/10.1016/j.jseaes.2014.03.012.

References

Arnold, M., Merchel, S., Bourlès, D.L., Braucher, R., Benedetti, L., Finkel, R.C., Aumaître, G., Gottdang, A., Klein, M., 2010. The French accelerator mass spectrometry facility ASTER: improved performance and developments. Nucl. Instrum. Methods Phys. Res. Sect. B 268, 1954–1959.

Beaumont, C., Kooi, H., Willett, S., 2000. Coupled tectonic-surface process models with applications to rifted margins and collisional orogens. Geomorphol. Global Tectonics, 29–55.

Beyssac, O., Simoes, M., Avouac, J.P., Farley, K.A., Chen, Y.G., Chan, Y.C., Goffé, B., 2007. Late Cenozoic metamorphic evolution and exhumation of Taiwan. Tectonics 26, TC6001, doi:10.1029/2006TC002064.

Bierman, P., Steig, E.G., 1996. Estimating denudation using cosmogenic isotope abundances in sediment. Earth Surf. Proc. Land. 21, 125–139.

Braucher, R., Merchel, S., Borgomano, J., Bourlès, D.L., 2011. Production of cosmogenic radionuclides at great depth: a multi element approach. Earth Planet. Sci. Lett. 309 (1), 1–9.

Brown, E.T., Edmond, J.M., Raisbeck, G.M., Yiou, F., Kurz, M.D., Brook, E.J., 1991. Examination of surface exposure ages of Antarctic moraines using in situ produced ^{10}Be and ^{26}Al. Geochim. Cosmochim. Acta 55, 2269–2283.

Brown, E.T., Stallard, R.F., Larsen, M.C., Raisbeck, G.M., Yiou, F., 1995. Denudation rates determined from the accumulation of in situ-produced ^{10}Be in the Luquillo Experimental Forest, Puerto Rico. Earth Planet. Sci. Lett. 129, 193–202.

Brown, E.T., Stallard, R.F., Larsen, M.C., Bourles, D.L., Raisbeck, G.M., Yiou, F., 1998. Determination of predevelopment denudation rates of an agricultural watershed (Cayaguas River, Puerto Rico) using in-situ-produced ^{10}Be in river-borne quartz. Earth Planet. Sci. Lett. 160, 723–728.

Byrne, T., Chan, Y.C., Rau, R.J., Lu, C.Y., Lee, Y.H., Wang, Y.J., 2011. The arc-continent collision in Taiwan. In: Brown, D., Ryan, P.D. (Eds.), Arc-Continent Collision. Frontiers in Earth Sciences, pp. 213–245, 10.1007/978-3-540-88558-0_8.

Chen, R.-F., Chan, Y.-C., Angelier, J., Hu, J.-C., Huang, C., Chang, K.-J., Shih, T.-Y., 2005. Large earthquake-triggered landslides and mountain belt erosion: the Tsaoling case, Taiwan. C. R. Geoscience. 337, 1164–1172.

Chen, C.H., Ho, H.C., Shea, K.S., Lo, W., Lin, W.H., Chang, H.C., Huang, C.H., Lin, C.W., Chen, G.H., Yang, C.N., Lee, Y.H., 2000. Geologic Map of Taiwan (1/500000): Central Geological Survey. Ministry of Economic Affairs, Taipei, Taiwan.

Ching, K.E., Hsieh, M.L., Johnson, K.J., Chen, K.H., Rau, R.J., Yang, M., 2011. Modern vertical deformation rates and mountain building in Taiwan from precise leveling and continuous GPS observations, 2000–2008. J. Geophys. Res. 116, B08406.

Chmeleff, J., von Blanckenburg, F., Kossert, K., Jakob, D., 2010. Determination of the ^{10}Be half-life by multicollector ICP-MS and liquid scintillation counting. Nucl. Instrum. Methods Phys. Res. Sect. B 268, 192–199.

Codilean, A.T., Fenton, C.R., Fabel, D., Bishop, P., Xu, S., 2014. Discordance between cosmogenic nuclide concentrations in amalgamated sands and individual fluvial pebbles in an arid zone catchment. Quaternary Geochronology. 19, 173–180.

Cruz, L., Malinski, J., Wilson, A., Take, W.A., Hilley, G., 2010. Erosional control of the kinematics and geometry of fold-and-thrust belts imaged in a physical and numerical sandbox. J. Geophys. Res. 115, B09404. http://dx.doi.org/10.1029/2010JB007472.

Dadson, S.J., Hovius, N., Chen, H., Dade, W.B., Hsieh, M.L., Willett, S.D., Hu, J.C., Horng, M.J., Chen, M.C., Stark, C.P., Lague, D., Lin, J.C., 2003. Links between erosion, runoff variability and seismicity in the Taiwan orogen. Nature 426, 648–651.

Dahlen, F.A., Suppe, J., 1988. Mechanics, growth and erosion of mountain belts. In: Clark, S.P., Burchfiel, B.C., Suppe, J. (Eds.), Processes in Continental Lithospheric Deformation. Geological Society of America Special Paper 218, pp. 161–178.

Davis, D., Suppe, J., Dahlen, F.A., 1983. Mechanics of fold-and-thrust belts and accretionary wedges. J. Geophys. Res. 88, 1153–1172.

Davison, A.C., Hinkley, D.V., 1997. Bootstrap Methods and their Applications. Cambridge University Press, p. 582.

Dunne, J., Elmore, D., Muzikar, P., 1999. Scaling factors for the rates of production of cosmogenic nuclides for geometric shielding and attenuation at depth on sloped surfaces. Geomorphology 27 (1–2), 3–12.

Efron, B., 1979. Bootstrap methods: another look at the Jackknife. Ann. Statis. 7, 1–26.

Efron, B., Tibshirani, 1986. Bootstrap methods for standard errors, confidence intervals, and other measures of statistical accuracy. Stat. Sci. 1 (1), 54–75.

Efron, B., Tibshirani, R.J., 1993. An Introduction to the Bootstrap. Chapman & Hall/CRC, Boca Raton, FL, 436 p.

Fuller, C.W., Willet, S.D., Hovius, N., Slingerland, R., 2003. Erosion rates for Taiwan mountain basins: new determinations from suspended sediment records and a stochastic model of their temporal variation. J. Geol. 111, 71–87.

Fuller, C.W., Willett, S.D., Fisher, D., Lu, C.Y., 2006. A thermomechanical wedge model of Taiwan constrained by fission-track thermochronometry. Tectonophysics. 425 (1–4), 1–24.

Gosse, J.C., Phillips, F.M., 2001. Terrestrial in situ cosmogenic nuclides: theory and application. Quatern. Sci. Rev. 20, 1475–1560.

Granger, D.E., Riebe, C.S., 2013. Cosmogenic nuclides in weathering and erosion. In: Drever, J.I. (Ed.), Surface and Ground Water, Weathering and Soils: Treatise on Geochemistry, vol. 5, second ed. Elsevier-Pergamon, Oxford, UK, p. 36 p (Chapter 14).

Granger, D.E., Kirchner, J.W., Finkel, R., 1996. Spatially-averaged long-term erosion rates measured from in situ-produced cosmogenic nuclides in alluvial sediment. J. Geol. 104, 249–257.

Granger, D.E., Lifton, N.A., Willenbring, J.K., 2013. A cosmic trip: 25 years of cosmogenic nuclides in geology. Geol. Soc. Am. Bull. http://dx.doi.org/10.1130/B30774.1.

Heimsath, A.M., Chappel, J., Finkel, R.C., Fifield, K., Alimanovic, A., 2006. Escarpment erosion and landscape evolution in southeastern Australia. In: Willet, S.D., Hovius, N., Brandon, M.T., Fisher, D.M. (Eds.), Tectonics, Climate, and Landscape Evolution. Geological Society of America Special Paper 398, pp. 173–190.

Hewawasam, T.F., von Blanckenburg, F., Schaller, M., Kubick, P.W., 2003. Increase of human over natural erosion rates in tropical highlands constrained by cosmogenic nuclides. Geology 3, 597–600.

Horng, C.S., Huh, C.A., Chen, K.H., Lin, C.H., 2012. Pyrrhotite as a tracer for denudation of the Taiwan orogeny. Geochem. Geophys. Geosyst. 13 (8), Q08Z47.

Hovius, N., Stark, C.P., Chu, H.-T., Lin, J.-C., 2000. Supply and removal of sediment in a landslide-dominated mountain belt: Central Range, Taiwan. J. Geol. 108, 73–89.

Kirchner, J.W., Finkel, R.C., Riebe, C.S., Granger, D.E., Clayton, J.L., King, J.G., Megahan, W.F., 2001. Mountain erosion over 10 yr, 10 k.y., and 10 m.y. time scales. Geology 29, 591–594.

Konstantinovskaia, E., Malavieille, J., 2005. Erosion and exhumation in accretionary orogens: experimental and geological approaches. Geochem. Geophys. Geosyst. 6, Q02006, doi:10.1029/2004GC000794.
Konstantinovskaya, E., Malavieille, J., 2011. Thrust wedges with décollement levels and syntectonic erosion: a view from analog models. Tectonophysics 502, 336–350.
Koons, P.O., 1990. 2-Sided orogen-collision and erosion from the sandbox to the Southern Alps, New-Zealand. Geology 18 (8), 679–682.
Korschinek, G., Bergmaier, A., Faestermann, T., Gerstmann, U.C., Knie, K., Rugel, G., Wallner, A., Dillmann, I., Dollinger, G., Lierse von Gosstomski, C., Kossert, K., Maiti, M., Poutivtsev, M., Remmert, A., 2010. A new value for the ^{10}Be half-life by heavy-ion elastic recoil detection and liquid scintillation counting. Nucl. Instrum. Methods 268, 187–191.
Lal, D., 1991. Cosmic ray labeling of erosion surfaces: in-situ nuclide production rates and erosion models. Earth Planet. Sci. Lett. 104, 424–439.
Lee, Y.H., 1976. Denudation of Taiwan Island since the Pleistocene epoch. J. Geol. 4, 105–107.
Li, F.C., Angelier, J., Chen, R.F., Hsieh, H.M., Deffontaines, B., Luo, C.R., Wu, T.T., Lin, M.C., 2005. Estimates of present-day erosion based on sediment transport in rivers: a case study in Taiwan. C. R. Geosci. 337, 1131–1139.
Liu, T.-K., 1982. Tectonic implications of fission track ages from the Central Range, Taiwan. Proceedings of the Geol. Soc. China 25, 22–37.
Liu, T.K., Chen, Y.G., Chen, W.S., Jiang, S.H., 2000. Rates of cooling and denudation of the Early Penglai Orogeny, Taiwan, as assessed by fission-track constraints. Tectonophysics 320, 69–82.
Liu, T.K., Hsieh, S., Chen, Y.G., Chen, W.S., 2001. Thermo-kinematic evolution of the Taiwan oblique-collision mountain belt as revealed by zircon fission track dating. Earth Planet. Sci. Lett. 186, 45–56.
Malavieille, J., 2010. Impact of erosion, sedimentation, and structural heritage on the structure and kinematics of orogenic wedges: analog models and case studies. Geol. Soc. Am. Acc. GSA Today 20 (1), doi:10.1130/GSATG48A.1.
McIntyre, G.A., Brooks, C., Compston, W., Turek, A., 1966. The statistical assessment of Rb–Sr isochrons. J. Geophys. Res. 71, 5459–5468.
Merchel, S., Herpers, U., 1999. An update on radiochemical separation techniques for the determination of long-lived radionuclides via accelerator mass spectrometry. Radiochim. Acta 84, 215–219.
Merchel, S., Arnold, M., Aumaître, G., Benedetti, L., Bourlès, D.L., Braucher, R., Alfimov, V., Freeman, S.P.H.T., Steier, P., Wallner, A., 2008. Towards more precise ^{10}Be and ^{36}Cl data from measurements at the 10–14 level: influence of sample preparation. Nucl. Instrum. Methods Phys. Res. Sect. B 266 (22), 4921–4926.
Molnar, P., 2009. The state of interactions among tectonics, erosion, and climate: a polemic. GSA Today 19 (7), 44–45.
Niemi, N.A., Oskin, M., Burbank, D.W., Heimsath, A.M., Gabet, E.J., 2005. Effects of bedrock landslides on cosmogenically determined erosion rates. Earth Planet. Sci. Lett. 237, 480–498.
Nishiizumi, K., Imamura, M., Caffee, M., Southon, J., Finkel, R., McAnich, J., 2007. Absolute calibration of Be-10 AMS standards. Nucl. Instrum. Methods Phys. Res. B 258, 403–413.
Palumbo, L., Hetzel, R., Tao, M., Li, X., 2009. Topographic and lithologic control on catchment-wide denudation rates derived from cosmogenic ^{10}Be in two mountain ranges at the margin of NE Tibet. Geomorphology 117, 130–142.
Portenga, E.W., Bierman, P.R., 2011. Understanding earth's eroding surface with ^{10}Be. GSA Today 21, 8. http://dx.doi.org/10.1130/G111A.1.
Sella, G.F., Dixon, T.H., Mao, A., 2002. REVEL: a model for recent plate velocities from space geodesy. J. Geophys. Res. 107 (B4), doi:10.1029/2000JB000033.
Selzer, C., Buiter, S.J.H., Pfiffner, O.A., 2008. Numerical modeling of frontal and basal accretion at collisional margins. Tectonics 27, TC3001, doi:10.1029/2007TC002169.
Shyu, J.B.H., Sieh, K., Chen, Y.-G., Liu, C.-S., 2005. Neotectonic architecture of Taiwan and its implications for future large earthquakes. J. Geophys. Res. 110, B08402.
Siame, L.L., Angelier, J., Chen, R.F., Godard, V., Derrieux, F., Bourlès, D.L., Braucher, R., Chang, K.J., Chu, H.T., Lee, J.C., 2011. Erosion rates in an active orogen (NE-Taiwan): a confrontation of cosmogenic measurements with river suspended loads. Quat. Geochronol. 6, 246–260.
Simoes, M., Avouac, J.P., Beyssac, O., Goffé, B., Farley, K.A., Chen, Y.G., 2007. Mountain building in Taiwan: a thermokinematic model. J. Geophys. Res. 112, B11405.
Stone, J.O., 2000. Air pressure and cosmogenic isotope production. J. Geophys. Res. 105, 23753–23759.
Strahler, A.N., 1952. Hypsometric (area-altitude) analysis of erosional topography. Geol. Soc. Am. Bull. 63, 1117–1142.
Suppe, J., 1981. Mechanics of mountain building and metamorphism in Taiwan. Mem. Geol. Soc. China 4, 67–89.
von Blanckenburg, F., 2005. The control mechanisms of erosion and weathering at basin scale from cosmogenic nuclides in river sediment. Earth Planet. Sci. Lett. 237, 462–479.
Ward, G.K., Wilson, S.R., 1978. Procedures for comparing and combining radiocarbon age determination: a critique. Archaeometry 20, 19–31.
Water Resources Agency, 2012. Ministry of Economic Affairs. <http://eng.wra.gov.tw/> (July 2012).
Water Resources Agency, 2014. Ministry of Economic Affairs, Precipitations in Taiwan. <http://eng.wra.gov.tw/ct.asp?xItem=48142&CtNode=7674> (January 2014).
Wendt, I., Carl, C., 1991. The Statistical Distribution of the Mean Squared Weighted Deviation. Chem. Geol. 86 (4), 275–285.
Whipple, K.X., Meade, B.J., 2004. Controls on the strength of coupling among climate, erosion, and deformation in two-sided, frictional orogenic wedges at steady-state. J. Geophys. Res. 109, F01011. http://dx.doi.org/10.1029/2003JF000019.
Willett, S.D., 1999. Orogeny and orography: the effects of erosion on the structure of mountain belts. J. Geophys. Res. 104, 28957–28981.
Willett, S.D., Fischer, D., Fuller, C., Yeh, E.C., Lu, C.Y., 2003. Erosion rates and orogenic-wedge kinematics in Taiwan inferred from fission-track thermochronometry. J. Geol. 31 (11), 945–948.
Willgoose, G., Hancock, G., 1998. Revisiting the hypsometric curve as an indicator of form and process in transport-limited catchment. Earth Surf. Proc. Land. 23 (7), 611–623.
Yamato, P., Mouthereau, F., Burov, E., 2009. Taiwan mountain building: insights from 2D thermo-mechanical modelling of a rheologically-stratified lithosphere. Geophys. J. Int. 176, 307–326.
Yanites, B.J., Tucker, G.E., Anderson, R.S., 2009. Numerical and analytical models of cosmogenic radionuclide dynamics in landslide-dominated drainage basins. J. Geophys. Res.: Earth Surf. 114, F01007.
You, C.F., Lee, T., Brown, L., She, J.J.S., Chen, J.C., 1988. ^{10}Be study of rapid erosion in Taiwan. Geochim. Cosmochim. Acta 52, 2687–2691.
Yu, S.B., Chen, H.Y., Kuo, L.C., 1997. Velocity field of GPS stations in the Taiwan area. Tectonophysics 274, 41–59.